Molecular phenomics of a high-calorie diet-induced porcine model of prepubertal obesity

Mariona Jové[1]*, Joan Tibau[2*#], José CE Serrano[1], Rebeca Berdún[1], María Rodríguez-Palmero[3], Maria Font-i-Furnols[2], Anna Cassanyé[1], Reyna Rodriguez-Mortera[1], Joaquim Sol[1], Helene Rassendren[1], Emma Fàbrega[2], Anna Crescenti[4,5] , Anna Castell [4,5] , Mònica Sabater[6,7,8] Francisco J Ortega[6,7,8] , Meritxell Martin-Gari[1], Raquel Quintanilla[9], Joaquim Puigjaner[3], Jose Antonio Moreno[3], Joan Prat[1], Lluis Arola[4,10], Josep Manuel Fernández-Real[6,7,8], Reinald Pamplona[1] and Manuel Portero-Otin[1#]

[1]NUTREN-Nutrigenomics Fisiopatologia Metabòlica, Universitat de Lleida-IRBLleida, E25196 Lleida, Spain; [2]Animal Breeding and Genetics Programme, Institute for Research and Technology in Food and Agriculture (IRTA), Finca Camps i Armet, E17121, Monells, Spain; [3]Laboratorios Ordesa S.L., Barcelona Science Park , 08028 Barcelona, Spain; [4]Nutrition and Health Unit, EURECAT-Technology Centre of Catalonia, Reus, Spain; [5]Nutrition and Health Research Group, EURECAT-Technology Centre of Catalonia, Reus, Spain; [6]CIBEROBN and Instituto de Salud Carlos III (ISCIII), Madrid, Spain; [7]Institut d'Investigació Biomédica de Girona (IdIBGi), Girona, Spain;[8]Department of Diabetes, Endocrinology and Nutrition (UDEN), Hospital of Girona "Dr Josep Trueta", Girona, Spain; [9] Product Quality Program, Institute for Research and Technology in Food and Agriculture (IRTA), Finca Camps i Armet, E17121, Monells, Girona,Spain;[10]Nutrigenomics Research Group, Department of Biochemistry and Biotechnology, Universitat Rovira i Virgili, Tarragona, Spain

*Both authors should be considered first authors

E-mail:

MJ: mariona.jove@mex.udl.cat, JT: joan.tibau@irta.cat, JCES: jceserrano@mex.udl.cat, RB: rebecaberdun@gmail.com, MRP: maria.rodriguez@ordesa.es, MFF: maria.font@irta.cat, AC: annakasa4@gmail.com, RRM: ln.reynarm@gmail.com, JS: jkim173@gmail.com, HR: ln.rassendren@gmail.com, EF: emma.fabrega@irta.cat, AC: anna.crescenti@eurecat.org, ACastell: anna.castell@eurecat.org, MS: msabater@idibgi.org, FJO: fortega@idibgi.org, MMG: meritxell.martin@udl.cat, RQ: Raquel.quintanilla@irta.cat, JP: Joaquim.puigjaner@ordesa.es, JAMM: joseA.moreno@ordesa.es, JPrat: joan.prat@mex.udl.cat, LA: lluis.arola@urv.cat, JMFR: jmfreal@idibgi.org, RP: reinald.pamplona@mex.udl.cat, MPO: manuel.portero@mex.udl.cat

Running title: ***Characterization of porcine early obesity***

Address for correspondence: [#]To whom correspondence should be addressed at Animal Breeding and Genetics Programme, Institute for Research and Technology in Food and Agriculture (IRTA), Finca Camps i Armet, E17121, Monells, Spain (Joan.Tibau@irta.cat) or Fisiopatologia Metabòlica, Universitat de Lleida-

IRBLleida, Edifici Biomedicina I, Avda Rovira Roure, 80 E25196 Lleida, Spain (manuel.portero@mex.udl.cat)

Grants

Supported by CDTI (Centro para el Desarrollo Tecnológico e Industrial, Spain), Project reference: IPT-20111008, and Generalitat de Catalunya grants 2017SGR1719 and 2017SGR696. Supported by ISCIII (Instituto de Salud Carlos III, Spain), Project reference: 17-00134 cofinanced by FEDER Funds *A way to make Europe*

Keywords

lipidomics; biomarkers; insulin resistance; preclinical models

Abstract

As obesity incidence is alarmingly rising among young individuals, we aimed to characterize an experimental model of this situation, considering the similarity between human and porcine physiology. For this reason, we fed prepubertal (63 days-old) Duroc breed females (n=20) either with a standard growth diet (3800 KCal/day) or one with a high-calorie content (5200 KCal/day) during 70 days. Computerized tomography, mass-spectrometry based metabolomics, and lipidomics, as well as peripheral blood mononuclear cell transcriptomics, were applied to define traits linked to high-calorie intake. Samples from a human cohort confirmed potential lipidomic markers. Compared to those fed a standard growth diet, pigs fed a high-calorie diet showed an increased weight gain (13%), much higher adiposity (53%), hypertriacylglyceridemia and hypercholesterolemia, in parallel to insulin resistance. This diet induced marked changes in the circulating lipidome, particularly in phosphatidylethanolamine-type molecules. Also, circulating specific diacylglycerol and monoacylglycerol contents correlated with visceral fat and intrahepatic triacylglycerol concentrations. Specific lipids associated with obesity in swine (mainly belonging to glycerophospholipid, triacylglyceride, and sterol classes) were also linked with obesity-traits in the human cohort, reinforcing the usefulness of the chosen approach. Interestingly, no overt inflammation in plasma or adipose tissue was evident in this model. The presented model is useful as a preclinical surrogate of prepubertal obesity in order to ascertain the pathophysiology interactions between energy intake and obesity development.

1. INTRODUCTION

Childhood obesity is linked to severe metabolic derangements in adult life [1]. Epidemiological studies reveal alarming rates of incidence of prepubertal and pubertal obesity [2], with its worrying impact on insulin resistance, development of type 2 diabetes, increased cardiometabolic risk, decreased bone health, as well as the psychological consequences of this derangement[3]. Therefore, the burden of increased caloric unbalance could seriously affect pubertal and postpubertal health[1].

Obesity is considered a multifactorial situation [4]. Under an evolutionary point of view, adipose tissue (AT) buildup in mammals can be a physiological response over changes in calorie availability, with a signaling role [5,6], which could be useful for homeostasis in an environment with energy availability oscillations. As such, increased fat content is not always linked to metabolic derangements [7]. The continuum between these two situations is still mostly unknown, leading to the uncertainty on why some individuals develop insulin resistance and enhanced cardiometabolic risk even with lack of AT build-up (metabolically unhealthy lean people) whereas other can cope with high amounts of adipose tissue (metabolically healthy obese) [8]. It is required an adequate characterization, at a molecular level, of the events between AT accumulation and its consequences, to fill this gap of knowledge.

In this line, available experimental models of obesity show some intrinsic limitations. For instance, rodents could exhibit increased obesity when placed in high-calorie intake, especially in the so-called cafeteria diet (e.g., an unbalanced diet with high fructose or high lipid content). Interestingly, due to the close physiological resemblance of porcine and human physiologies, specific cardiometabolic markers translate better in pigs than in rodent models. These include low HDL-cholesterol, increased LDL-cholesterol, coronary calcification, to name a few. Thus, in both primates and swine, lipoprotein metabolism is very similar to humans [9,10]. Therefore, unhealthy diets in these species are able to induce changes in lipid profiles associated with cardiometabolic risk, reproducing many changes present in humans [10,11]. Pigs are particularly suited for evaluating their lipid metabolism, based on the knowledge of genetic traits controlling them, and the possibility to monitor the buildup of AT by using clinical imaging systems as computed tomography (CT)[12,13].

Systems biology has helped to unravel the pathogenic role of specific fat depots in both humans and rodents. Among involved disciplines, proteomics, metabolomics, and lipidomics are closely interlaced with the phenotype, offering a dynamic view of the ongoing molecular changes. Metabolomics either focused on polar molecules or lipidomics (when lipids are extracted before the analyses), have the advantage of covering a high number of potential candidate biomarkers. When combined adequately with confirmatory techniques, they could disclose pathogenic pathways amidst generating novel hypotheses for diagnosis, prognosis, and therapeutics.

In this context, the present work aims to characterize molecular traits associated with the obesity induced by a high-calorie diet in prepubertal female pigs. This goal is achieved by combining an imaging platform based on CT evaluation of AT distribution, weight evolution, food intake with changes in circulating lipidome and metabolome, with a view of specific transcripts in the subcutaneous AT and in the transcriptome of the peripheral blood mononuclear cells (PBMCs). These later were chosen as they may share, at least partially, share the expression profile of different sets of genes with other tissues, including those that reflect metabolic responses[14–16]. Furthermore, the lipidomic changes were validated in a cohort of human subjects to confirm the robustness of these observations. Finally, these changes were compared with clinically validated biomarkers of obesity-related dyslipidemia with some of the suggested pathogenic pathways confirmed in adipose and liver tissues.

2. METHODS

All the experimental procedures with pigs, including management, traits recording, monitoring, and blood sampling, were approved by the Ethical Committee of the Institut de Recerca i Tecnologia Agroalimentàries (IRTA, Girona, Spain). In the case of human samples, these were obtained from the FLORINASH study cohort [17], and its institutional review board approved the study protocol, and all subjects provided informed

written consent. Briefly, we recruited 44 consecutive subjects. Inclusion criteria were age 30–65 years and acceptance to study procedures. Exclusion criteria were a systemic disease, infection in the previous month, chronic severe illness, ethanol intake >20 g/day, or use of medications that might interfere with insulin action. For comparison with porcine model-derived biomarkers, we recorded body to mass index (BMI) and homeostatic model assessment for insulin resistance (HOMA-IR). See supplemental Table 1 for clinical characteristics (supplemental data). Sources for chemicals are also presented in the extended Methods section (supplemental data).

2.1 Animals and treatments

A total of 21 female piglets from a high intramuscular fat Duroc pig line were used in the present study. Animals were born in 10 different litters (i.e., ten pairs of littermates) and were distributed randomly to one of the two diets (conventional diet for growth and western-type, see below). After weaning, piglets were transferred to the IRTA pig experimental test station and subjected to the same management procedures. From weeks 9 to 11, animals were adapted to a transition diet (Supplemental Tables 2 and 3). Subsequently, each of the sibling pairs was divided into the two dietary treatments: animals fed a conventional growth diet and animals fed a western-type diet with a high-calorie, high-sucrose and low fiber content (detailed composition and nutritional properties shown in supplemental Tables 4 and 5,). The experiment lasted until pigs reached 19 weeks of age when animals were sacrificed after an overnight fast, at IRTA experimental slaughterhouse compliance with all welfare regulations. Pigs were weighed individually at the beginning and every two weeks during the whole experiment, plus the day before slaughter. Daily feed intake (FI; kg/day) was recorded individually through theautomatic electronic feeding system HOKOFARM-IVO-G ® (Marknesse, The Netherlands): all animals are identified electronically and located in contiguous pens in the same barn (with 10 – 11 animal groups of littermates). Each pen is provided with an automatic feeding recording system (system HOKOFARM-IVO-G ®), allowing full control

of individual voluntary *ad libitum* feed intake. Each particular meal intake (10 to 20 per day) is recorded, and the full dailyfeed ingested amount is computed for each animal (as well as the number and duration of meals). Blood samples for biochemical and transcriptome analyses were taken from fasted animals immediately before sacrifice. After slaughtering, pelvic-renal fat (flare fat) was removed and weighted.

2.2 Computed tomography scanning and image analysis

All pigs were CT-scanned one week before sacrifice employing the General Electric HiSpeed ZX/I (Fairfield, CN, USA) equipment located at IRTA in Monells (Girona,Spain) as explained in [12] and images were analyzed using software VisualPork [18,19] developed by the University of Girona and IRTA. See Figure 1A and 1B as an example of employed images. See the extended Methods section (supplemental data) for further description.

2.3 Biochemical analyses and western blot

Serum lipids and other conventional biochemical variables were measured in fasted animals in blood obtained immediately before sacrifice by using commercial kits, including triacylglycerides, total cholesterol, LDL- cholesterol, HDL cholesterol, and glucose, as described previously [20]. Plasma interleukin concentrations were measured using Millipore multiplex kits for porcine samples (Millipore, Barcelona, Spain) according to manufacturer instructions. Plasma insulin content was measured using a commercial ELISA kit (Abcam, Cambridge, UK). Total lipids were extracted from the liver (80 mg) and dried feces (100 mg) of the pigs and were quantified using the methods previously described [21]. In the liver and feces samples, triglycerides and cholesterol were quantified by colorimetric kits (QCA, Barcelona, Spain). Western blot analyses of tissues were performed as described[20] and explained in the extended Methods section

(supplemental data), using as primary and secondary antibodies those listed in supplemental Table 6 (supplemental data).

2.4 Untargeted lipidomic analyses of plasma

Plasma lipidomic analysis was based on a previously validated method [22]. Internal standards (listed in supplemental Table 7), lipid extraction, and lipidomic techniques are explained in the extended Methods section (supplemental data). Lipid extracts were subjected to liquid chromatography coupled to mass spectrometry (LC-MS) using an Agilent UPLC 1290 coupled to the Q-TOF MS/MS 6520 (Agilent Technologies, Barcelona, Spain) based on a previously published method [23].

2.5 Untargeted metabolomics analyses of serum

The metabolomic analyses of serum extracts were performed by LC-MS and further explained in the extended Methods section (supplemental data).

2.6 Peripheral blood monocyte cells (PBMC) transcriptomics and AT leptin expression

PBMCs transcriptomics was done of (n=7 from each group) at the Centre for Omic Sciences (Reus, Spain) by using the Porcine (V2) Gene Expression Microarray, 4x44K (Agilent Technologies) following manufacturer's instructions. AT mRNA expression in the subcutaneous depot was quantified as previously described [24] by using real-time PCR in a LightCycler 480 Real-Time PCR System (Roche Diagnostics) using TaqMan® technology suitable for relative gene expression quantification. Both methods are further developed in the extended Methods section (supplemental data).

2.7 Data processing, Network, and Statistic Analyses

In the case of lipidomics and metabolomics, the MassHunter Data Analysis Software (Agilent Technologies) was used to collect the results and the MassHunter Qualitative Analysis Software (Agilent Technologies) to obtain the molecular features of the samples, representing different, co-migrating ionic species of a given molecular entity (i.e., ion adducts) using the Molecular Feature Extractor algorithm (Agilent Technologies)

[25]. This algorithm uses the accuracy of the mass measurements to group related ions (based on the charge-state envelope, isotopic distribution, and the presence of different adducts and dimers/trimers) assigning multiple species (ions) to a single compound referred to as a feature. Finally, the MassHunter Mass Profiler Professional Software (Agilent Technologies) was used to perform a non-targeted analysis over the extracted features. Only shared features (found in at least 75% of the samples of the same condition) were taken into account to correct for individual bias. In the case of non-targeted lipidomics, proposed annotation by lipid class is based on exact mass, isotopic distribution, and retention time of lipid family standards, so fatty acid distribution offered is one of the potential combinations leading to the same number of carbons and unsaturations.

In the case of non-targeted metabolomics, the identification of detected compounds with significant differences was performed based on the exact mass, the adduct formation, and the isotopes relative abundance and spacing using the Metlin/PCDL database and Molecular Formula Generation software (Agilent Technologies).

In case of lipidomics, after log transformation and auto-scaling of variables, the masses representing significant differences by Student's t-test ($p < 0.05$ with false discovery rate correction) were searched against the LIPID MAPS database (The LIPID MAPS Lipidomics Gateway, http://www.lipidmaps.org/, February 2018) (exact mass ppm < 20).

All other analyses were performed either with the SAS software ver. 9.4 (SAS Institute Inc., Cary, NC, USA), with the Prism ver 7 (GraphPad Software, La Jolla, CA, USA) or with the SPSS software ver 24 (IBM Corp, Armonk, NY, USA). Non-linear fit (exponential growth equations; $Y=Y0*\exp(k*X)$) lines in the graphs correlating two variables were produced with the Prism software. Multivariate statistics (Hierarchical Clustering, PCA, and PLS-DA analyses) were done using the Metaboanalyst platform software [26]. Gene enrichment and induced network module analyses were performed in the

ConsensusPathDB platform [27]using as input genes*agtpbp1, fcrl4,herc4,egr2, loc780435, loc100622399, loc100621244, krt18, ly49, pth, kctd14, ppp1r36, and trim46.* The same list was also explored with the Genemania platform[28], using Homo sapiens (human) as the reference and searching for its potential relationship with genes in lipid metabolism *pemt* and *srbep1*.

3. RESULTS

As expected, animals under the western-type regime increased weight in a significant amount (Table 1). However, despite these animals ingested near 37% more calories per day, the difference in weight did not reach these changes, only achieving 13% more weight. This ponderal change was also associated with an increased fecal fat content (in cholesterol and triacylglyceride content). Nonetheless and despite these data pointing for a trend for fecal lipid loss, adiposity, measured by CT imaging, increased sharply, reaching *ca* two fold increases in AT derived parameters, such as relative fat volume and pelvic-renal fat content. Concerning biochemical consequences associated with obesity, animals under the high-calorie regime increased plasma cholesterol significantly, its subfractions, and triacylglyceridemia in parallel to insulin resistance (HOMA-IR, *ca* 43%, $p<0.01$), suggesting an early impairment in glucose homeostasis (Table 1).

To enhance the knowledge of the molecular basis of this phenotype, we performed a non-targeted lipidomic analysis in plasma samples. This approach shows that prepubertal obesity changed the amounts of 187 molecules (p values ranging between 1.49E-20 and 0.05; Supplemental dataset 1), with very significant changes in 23 compounds (FDR <0.1). These comprised 4 phosphatidylethanolamines and a cerebroside, among the top markers. Hierarchical clustering resulted in a clear separation between the two lipidomes using the 25 most statistically significant molecules (Figure 1C) with a PLS-DA model (Figure 1D) with high accuracy (71%, with

R2=0.92 in a one model component, Supplemental Figure 1). Variable importance in projection scores reinforced the importance of several phosphatidylethanolamine and phosphatidylserine molecules in the first component, with a cerebroside, a monoacylglycerol and a sterol related molecule among these discriminating features (Supplemental Figure 1).

We studied if specific circulating lipids correlated with individual parameters affecting final weight since the high-calorie intake impacted differently on each individual (e.g., variances higher than 10% in the final weight, Table 1). Concerning calorie consumption, 218 molecules correlated significantly with calorie intake (p values ranging between 7.61E-7 and 0.05, Spearman rank correlation between absolute values between 0.85 and 0.42, Supplemental Dataset 2). Among these, three phosphatidylethanolamines were among the top targets correlating with calorie intake (Figure 1D). Interestingly, several molecules also correlated with AT content (226 molecules, with p values between 6.8 E-6 and 0.05, Spearman rank absolute correlation values between 0.81 and 0.43, Supplemental Dataset 3). Besides phosphatidylethanolamines, other lipids showed a high correlation, such as a monoglyceride and a cerebroside (Figure 1E). The targets correlating with pelvic-renal AT depot abundance were different from those of total fat, suggesting the fact that non-subcutaneous fats constitute depots with unique pathophysiological traits. Thus, 169 different molecules correlated with pelvic-renal depot abundance (p values between 5.9E-5 and 0.05, Spearman rank absolute correlation values between 0.76 and 0.43, Supplemental Dataset 4). Though phosphatidylethanolamines were correlated as well, top molecules belonged to cholesteryl esters and to phosphatidylserine (Figure 1F).

Interestingly and independently from lipidomic changes in plasma, a partial least square discriminant analyses (PLS-DA) model encompassing AT depots and lipidemia variables ((plasma, liver, and LDL cholesterol) exhibit a high accuracy (Supplemental Figure 2A).

Clustering analyses showed that not all the adipose tissue depots clusterized together, with pelvic-renal fat being associated with lipidemia variables, (Supplemental Figure 2B). In contrast, total fat and subcutaneous fat depot were more closely associated with calorie intake and final weight. Variable importance in projection (Supplemental Figure 2C) showed that the most influential variables were calorie intake, total fat, and subcutaneous fat percentages. Permutation tests demonstrated the robustness of this model (Supplemental Figure 2D).

As LDL cholesterol was also affected by western-typeregime, we evaluated potential lipidomic markers linked to this biochemical trait. Interestingly, these differed from those correlated with other biochemical characteristics. Thus, 165 molecules correlated with LDL cholesterol concentrations (p values between 2.5 E-5 and 0.05, Spearman rank correlation absolute values between 0.71 and 0.43, Supplemental DataSet 5). These molecules comprised a specific phosphatidylethanolamine (different from the one correlated with fat contents) and several unknown lipids (Supplemental Figure 3).

As increased fasting glycemia and HOMA-IR (despite no overt hyperinsulinemia) were evidenced in this model of prepubertal obesity, we searched for lipidomic markers of insulin resistance. Insulin concentrations were correlated with 90 different lipids (p values between 0.0003 and 0.05, Spearman rank absolute correlation values between 0.68 and 0.43, Supplemental Dataset 6). Specific molecules comprised a phosphatidic acid and a lactosyl-ceramide (Figure 2A). Similarly, a total of 77 molecules correlated with HOMA-IR (p values between 0.0002 and 0.05, Spearman rank absolute correlation values between 0.75 and 0.46, Supplemental Dataset 7). These included specific triacylglycerides and sphingolipids (Figure 2A). Insulin acts on adipogenesis via specific effectors such as SREBP1 [29]. Although we did not observe overt hyperinsulinism but insulin resistance, we evaluated insulin-dependent signals in adipose tissues of this model. The results demonstrate anatomic differences in the impact of a high-calorie diet

316 in insulin signaling modules of adipose tissue. Both adipose tissues from pelvic-renal
317 and omental locations showed a significantly increased amount of SREBP1c, while
318 subcutaneous and omental ATs locations showed decreased Glut4 levels, consistent
319 with insulin resistance (Figure 2B). Of note, AT in the pelvic-renal location did not show
320 detectable levels of Glut4 (data not shown), but Glut2. We also evaluated the expression
321 of specific mRNs in the subcutaneous depot (Supplemental Table 8). We studied which
322 of the circulating lipids correlated with leptin expression since leptin levels mirror
323 adipogenesis in subcutaneous depot (significantly increased by evaluation of its mRNA
324 content in 186%, $p<0.00001$). The results demonstrate significant associations of *leptin*
325 mRNA levels in subcutaneous AT and 138 lipids in plasma (p values between 4.92E-05
326 and 0.049, Spearman rank correlation absolute values between 0.76 and 0.43,
327 Supplemental Dataset 8). These include specific phosphatidylethanolamine and
328 triacylglycerides (Figure 2C). The specificity of the lipidomic changes associated with
329 insulin signaling is evidenced by the lack of common lipidomic correlations with leptin
330 mRNA and very low common correlations with fat content (Figure 2D).
331 As the liver is also a target of obesity, we evaluated the potential occurrence of hepatic
332 steatosis in this model. The results show that the western-type diet in this model did not
333 change neither triacylglycerides nor cholesterol content (Supplemental Figure 4).
334 Despite no significant changes were measured in phosphorylated-IRS1 (Ser 307, Ser
335 1101) or in phosphorylated c-Jun (Ser 73) (supplemental Figure 4) decreased Glut2
336 content potentially marked incipient insulin resistance, (Figure 3A), with some circulating
337 lipids correlating significantly with changes in hepatic fat content. Thus, 123 molecules
338 correlated with hepatic triacylglyceride content (p values between 1E-4 and 0.05,
339 Spearman rank absolute correlation values between 0.74 and 0.43, Supplemental
340 Dataset 9). These comprised a diacylglycerol and a phosphatidic acid (Figure 3B).
341 Plasma species correlating with liver triacylglyceride content are quite specific (Figure
342 3C). Noteworthy, changes in glucose transporters did not affect, at this stage, skeletal
343 muscle (Supplemental Figure 5).

In line with the moderate impact of high calorie in this model, plasma values of measured interleukins did not demonstrate overt inflammation (Supplemental Table 9). However, statistically significant correlations were present between circulating lipids and selected interleukins, including IL-1a, IL-1b, and IL-18 (Supplemental figure 6, supplemental Dataset 10 for correlated lipids). These lipids comprised specific phosphatidylethanolamines, triacylglycerides, and tocopherol derivates.

To evaluate whether this model could be of usefulness in human obesity, we compared the results with those obtained from plasma lipidomic analyses of a human cohort. As Figure 4 shows, there is a consistent overlap between the behavior of selected biomarkers of obesity and its metabolic consequences between these two species. Thus, selected phospholipid molecules (phosphatidylserine (21:0, 22:0), sterols (5-cholestan-3-one), and unidentified lipids correlated significantly both with BMI in humans and with fat abundance in pigs. Interestingly, other lipids also correlated with HOMA-IR in both species, underlying the usefulness of the chosen model. The same behavior was observed for correlations between cerebroside D, N-(11Z,14Z-eicosadienoyl)-ethanolamine, TG (16:0/16:1(9Z)/16:1(9Z)) and BMI (R^2=0.31, p<0.0001; R^2=0.09, p<0.03; R^2=0.12, p<0.02 after Pearson correlation analyses), as presented in Supplemental Figure 7.

To further characterize the impact of western-type diet in the porcine model, we also analyzed changes in the aqueous soluble phase of serum and explored changes in the PBMC transcriptome profile. Globally speaking, the number of differential features was much lower comparing the aqueous extracts with those of organic solvents (Supplemental Table 8). When aggregating these changes of metabolites into pathways, these defined a network that comprised variations in metabolites belonging to branched-chain amino acids (BCAA), central carbon metabolism, and pantothenate and coenzyme

A synthesis (Figure 5). Changes in PBMC transcriptome (Supplemental Dataset 11), when mapped, revealed two main networks affected by high-calorie intake (Supplemental Figure 8). One was related to *EGR2*, and the other was mainly paired with *KRT18* and *RAAR* genes. The functional annotation of these genes clustered in 4 different enriched neighborhood-based tests ($p<0.001$), which included *SUV420H2, DTX4, DTX1,* and *USP49* (Supplemental Figure 9). We also evaluated the potential network proximity between genes in PBMC transcriptome and key genes in metabolism, *SREBP1,* and *PEMT*. These two later belonged to the network of expression of *KRT18* and *EGR2* (Supplemental figure 10).

4. DISCUSSION

The present work reinforces the usefulness of high-calorie regimes in porcine models to evaluate obesity pathophysiology [30,31]. Interestingly, we found that the body weight gain induced by high calorie, although significant, was not proportional to calorie intake. This fits with the notion that weight gain and calorie intake are not linear[32]. In rats, physical activity, among other factors, could divert dietary fats towards oxidation and less to the storage, in a manner associated with de novo lipogenesis in adipose tissue, as well as increases in skeletal muscle uptake and oxidation of lipids [33]. This metabolic switch seems not uncommon in swine [34]. Of note, fat content increased in the high-calorie group. In any case, our model can be viewed as an early obesity model, with some traits of metabolic syndrome. This resemblance with human pathology has been already described for domestic pigs under similar, high-fat regimes, where short term interventions led to weight gain and dyslipidemia, but not tovert insulin resistance or metabolic syndrome[35]. Several factors may explain the relatively small metabolic impact in the current porcine model in comparison to other reported porcine models, including the age of the individuals, the lack of a large amount of refined sugars (fructose or sucrose), in comparison to other diets inducing obesity in porcine models, the specific breed or the length of treatment.

In order to characterize the molecular traits explaining these obesity-related changes, we performed non-targeted lipidomic analyses of plasma samples. For the sake of brevity, we will limit mainly the discussion of those results obtained after FDR correction. The results suggest the role of specific phosphatidylethanolamines as potential obesity circulating biomarkers at a molecular level. One of the most differential identifiable markers is a dimethylphosphatidylethanolamine. These products are intermediates in the liver synthesis of phosphatidylcholine *de novo* biosynthesis through methylation of phosphatidylethanolamine, especially relevant when choline is deficient in diet [36]. This conversion is catalyzed by the enzyme phosphatidylethanolamine *N*-methyltransferase (PEMT), whose activity is regulated by adenosylmethionine and phosphatidylethanolamine levels. Since this activity is essential for VLDL secretion, we hypothesize that increased levels of the dimethylphosphatidihylethanolamine detected could be a proxy for increased PEMT activity in the liver and VLDL secretion, required for exporting hepatic lipids towards their adipose depot. PEMT loss renders protection over diet-induced obesity[37], suggesting that in our model of obesity, this activity is increased. Noteworthy, PEMT expression and colocalization are related with *EGR2* and *KRT18*, as pathway analyses show. Other lipids significantly related to energy intake, were specific phosphatidylethanolamine (PE) with long fatty acids. These findings could go in line with data from lipidomic analyses of plasma from overweight and obese healthy individuals [38]. In these analyses, other PE species appeared to be relevant components of a plasma lipidomic signature of obesity. Interestingly, in other cohorts of patients with prediabetes and diabetes, increased PE levels were noted as well [39]. In this context, these were interpreted as a source for inflammatory eicosanoids, which may be as well our case, as one of the potential fatty acids present in these PE is arachidonic acid. Other works revealed an association of a specific PE, containing 40:6 fatty acids, with insulin resistance in human individuals[40].

Reinforcing the validity of porcine lipid metabolism in the context of human obesity, increases in specific PE-related species[41], such as plasmalogens, were observed in obese subjects. Plasmalogens are part of an antioxidant response towards increased oxidative stress with high-calorie intake. Nonetheless, several phospholipids (phosphatidylserine and sterol molecules) correlated with BMI and AT abundance in both species using the same methodological approach.

Other lipids were significantly associatedwith adiposity, measured by CT imaging. Thus, increases in a long chain monoacylglycerol were detected. In mice, the deletion of one of the enzymes linked to monoacylglycerol degradation, monoacylglycerol lipase, leads to increased concentrations of monoacylglycerol and resistance to obesity, as well as delayed lipid absorption [42]. The increased levels detected here may be viewed as a potential homeostatic downregulation of monoacylglycerol lipase activity. Another lipid showing a similar behavior with adiposity, cerebroside D, has been reported to be a potent immunomodulatory agent in mice models of experimental colitis[43]. Furthermore, glucocerebrosides afford protection over the metabolic syndrome induced by leptin loss in mice [44]. It is known that structurally related compounds, such as glucosylated ceramides and ceramides, play critical roles in insulin resistance, which has an inflammatory background [45], therefore increased cerebroside D might be viewed as a compensatory response to avoid the high-energy induced inflammatory burden. Of note, cerebroside D was also found in the humane cohort used for the translational applicability of the model, thereby reinforcing its potential importance in obesity pathophysiology.

In line with the pathophysiological relevance of the location of adipose tissue depots [24], the lipids that correlated with total adiposity were different from those correlating with the amount of pelvic-renal fat depot, a typical visceral location. Cholesteryl ester 18:3, associated with the amount of this AT, has been previously shown to be decreased in a murine model of obesity [46]. However, and reinforcing the similarity of porcine

456 models with humans, a sizeable lipidomic survey revealed a significant association of
457 cholesteryl esters with body mass index in humans[47]. The other lipid, a
458 phosphatidylserine, has not been previously related to obesity, but instead to
459 preeclampsia in humans[48]. Glycerophosphoserines play vital structural roles in cell
460 membranes [49], where they may regulate oxidative stress responses and apoptosis,
461 but so far, it was not associated with high energy intake. Of note, a glycerophosphoserine
462 was found among the biomarkers shared between the porcine study and the humane
463 cohort. These lipids have been linked recently to changes in postprandial lipidome after
464 physical activity in humans with type 2 diabetes [50].
465
466 Finally, phosphatidic acid and diacylglycerol were associated with triacylglyceride
467 content in the liver. Interestingly, diacylglycerol species were as well noted as relevant
468 biomarkers by overfeeding experiments in humans[41], and phosphatidic acid increases
469 considerably during diet-induced nonalcoholic fatty liver disease [51]. Further, these data
470 reinforce the usefulness of plasma lipidomic signature for minimally invasive monitoring
471 of liver status [52].
472
473 Even though we detect no changes in some circulating surrogates of insulin resistance
474 (such as fructosamine), we were able to detect molecular markers of adipose tissue and
475 liver insulin resistance. Sphingolipids were found among the measured markers
476 correlating with HOMA-IR and insulin. This relationship agrees with the well-described
477 role of ceramide signaling in human obesity-related insulin resistance (reviewed in[53]).
478 Globally, this association would reinforce the validity of this model in evaluating the
479 pathophysiology of obesity-related metabolic rearrangements. In line with this, and
480 similar to humans, fat depots showed a location-specific response to high-calorie diet in
481 the expression of glucose transporters and adipogenic proteins (as SREBP-1c). Further,
482 AT leptin expression was increased, in line with adipose tissue expansion.
483

The changes in circulating metabolome and transcriptome also support the usefulness of the model: changes in BCAA metabolism have been described in several clinical studies, demonstrating that its alteration could predict diabetes development[54]. These variations can be associated with ongoing inflammation and with mitochondrial alterations, though in our model, no evidence for inflammation was found. Interestingly, we also found pieces of evidence for altered pantothenic-related metabolic pathways in our model of obesity. This concept fits with recently described findings in Yucatan mini-pigs fed with a high-fat,high-sucrose diet for two months, also reporting amino acid metabolism changes, reduced capacities of BCAA transamination, and alteration in pantothenic metabolism [55]. In line with these results, transcriptomic changes in PBMC agree with previous data in humans. Thus, previous data in adipocytes reveal that EGR function, related to one of the pathways found in the transcriptome, is required to enhance triacylglyceride depot [56]. In mice, EGR represses FOXC2 expression and is required for the development of obesity under high-calorie intake. Of note, it is known that insulin inhibits EGR expression in peripheral cells [57]. Therefore, one could see EGR changes in PBMC as early markers for insulin dysfunction. Similarly, KRT18 has been invoked as a biomarker for obesity-related hepatic dysfunction in obese adolescents [58], so our finding of its change in this model would support its use as a preclinical model of human pubertal obesity. Functional neighborhood analyses revealed ubiquitin ligases DTX4 and DTX1 and the methyltransferase SUV420h2 as potential nodes of interest, as previously reported data on adipocyte differentiation and diet-induced obesity reveals [59,60]. These results reinforce the usefulness of PBMC transcriptome analyses in this model.

We assume, as limitations of the present work, that only using a single-gender could hinder the application of those results to human pathophysiology, especially those related to the influence of sex hormones in lipid metabolism. However, the fact that many markers were replicated in a completely independent fashion in a human cohort (with

both genders and older age) with obesity supports the usefulness of the chosen approach. Further, we acknowledge that a more thorough examination of this cohort (e.g., at older ages) would be advantageous to define the unique features of prepubescent obesity in this context. Based on the comparative analyses with the human cohort, we propose that those markers in common with consolidated obesity could show some promise in the pathophysiological research of increased AT depots. In contrast, those not in common with humans could be either derived from specific porcine metabolism, from younger age of examined specimens, or related to resilience towards pathological effects of AT buildup. Although the number of calories consumed is much higher in comparison with humans (both in the conventional and in the western-type diet), the experimental group exhibited a marked increase in daily intake of calories. Further, on the qualitative side, experimental diets modeling western-type diets include those such as the “cafeteria diet” with high-calorie content, high sucrose, and fat contents, with lower protein amounts [61,62]). These also include high fat with high cholesterol content[63]. Other authors also include a low fiber component[64]. Despite this diversity, our model shows most of these traits, reproducing the western-type dietary patterns. Further, lipidomic identification proposed aims at level 2, according to the Metabolomics Standards Initiative [65], so they are putatively annotated compounds (e.g., without chemical reference standards, based upon physicochemical properties and spectral similarity with public/commercial spectral libraries). Therefore, some of these reported metabolites might vary in their final identification., Noteworthy, our model of prepubescent obesity may be useful for the evaluation of the biological basis of metabolically healthy obesity. A high proportion of obese children are metabolically fit [66]in a close relationship with a higher propensity of subcutaneous fat accumulation. Our model shows both a high subcutaneous fat accumulation concurrently with a non-marked inflammatory response. Further, some of the circulating lipids correlate with physiological responses to AT expansion (e.g., leptin expression), while some others correlate with pathological traits (inflammatory markers or the HOMA-IR). This fact

reveals the mixed nature of lipidomic responses to western-type diet in this model, but we think that the reported data could be of interest in order to get the full profit of this model as a *bona fide* preclinical surrogate of pubertal obesity.

COMPETING INTERESTS

No competing interests declared.

FUNDING

Supported by CDTI (Centro para el Desarrollo Tecnológico e Industrial, Spain), Project reference: IPT-20111008, and Generalitat de Catalunya grants 2017SGR1719 and 2017SGR696. Supported by ISCIII (Instituto de Salud Carlos III, Spain), Project reference: 17-00134 cofinanced by FEDER Funds *A way to make Europe*

AUTHORS CONTRIBUTIONS

Conceptualization:J.T.,M.R.P,J.Pu.,J.Pr,M.P.O.

Methodology:M.J.,J.T.,M.F.F.,J.Pu,M.P.O.

Software:M.F.F.,J.T.,J.S., E.F.

Validation:R.B.,L.A., M.M.G.,J.M.F.R.

Formal analysis:M.J., J.C.E.S.,J.S.,A.Cr., A. Cast,M.S.,F.J.O.,L.A., J.M.F.R.

Investigation:M.J., J.C.E.S.,A.C.,H.R., A. Cr.,R.R.M., A.Cast.,M.S.,R.Q.

Resources:M.R.P., J.T.,R.Q.,J.M.F.R.

Data curation:A.C., J.S., H.R.,E.F.

Writing – original draft preparation:M.P.O.,J.A.M.,J.T.

Writing – review, and editing:R.Q.,J.A.M., J. Pr, J.M.F.R., R.P., M.P.O

Visualization:R.P,M.F.F., E.F.

Project administration:J.T.,M.R.P

Funding acquisition:J.T.,M.R.P.,J.M.F.R., M.P.O

SUPPLEMENTARY DATA

All supplementary figures and tables are present as supplementary information

available at Journal's website. Supplemental Datasets are freely available under a CC BY 4.0 license at Figshare.com website at https://figshare.com/s/bf91f3332d1f6d9d4f26

REFERENCES

[1] Liang Y, Hou D, Zhao X, Wang L, Hu Y, Liu J, et al. Childhood obesity affects adult metabolic syndrome and diabetes. Endocrine 2015;50:87–92. doi:10.1007/s12020-015-0560-7.

[2] Cunningham SA, Kramer MR, Narayan KMV. Incidence of childhood obesity in the United States. N Engl J Med 2014;370:403–411. doi:10.1056/NEJMoa1309753.

[3] Deckelbaum RJ, Williams CL. Childhood obesity: the health issue. Obes Res 2001;9 Suppl 4:239S–243S. doi:10.1038/oby.2001.125.

[4] Procter KL. The aetiology of childhood obesity: a review. Nutr Res Rev 2007;20:29–45. doi:10.1017/S0954422407746991.

[5] Trayhurn P, Beattie JH. Physiological role of adipose tissue: white adipose tissue as an endocrine and secretory organ. Proc Nutr Soc 2001;60:329–339. doi:10.1079/PNS200194.

[6] Trayhurn P, Bing C. Appetite and energy balance signals from adipocytes. Philos Trans R Soc Lond B, Biol Sci 2006;361:1237–1249. doi:10.1098/rstb.2006.1859.

[7] Bervoets L, Massa G. Classification and clinical characterization of metabolically "healthy" obese children and adolescents. J Pediatr Endocrinol Metab 2016;29:553–560. doi:10.1515/jpem-2015-0395.

[8] Phillips CM. Metabolically Healthy Obesity: Personalised and Public Health Implications. Trends Endocrinol Metab 2016;27:189–191. doi:10.1016/j.tem.2016.02.001.

[9] Litten-Brown JC, Corson AM, Clarke L. Porcine models for the metabolic syndrome, digestive and bone disorders: a general overview. Animal 2010;4:899–920. doi:10.1017/S1751731110000200.

[10] Miller ER, Ullrey DE. The pig as a model for human nutrition. Annu Rev Nutr 1987;7:361–382. doi:10.1146/annurev.nu.07.070187.002045.

[11] Hamamdzic D, Wilensky RL. Porcine models of accelerated coronary atherosclerosis: role of diabetes mellitus and hypercholesterolemia. J Diabetes Res 2013;2013:761415. doi:10.1155/2013/761415.

[12] Carabús A, Gispert M, Brun A, Rodríguez P, Font-i-Furnols M. In vivo computed tomography evaluation of the composition of the carcass and main cuts of growing pigs of three commercial crossbreeds. Livest Sci 2014;170:181–192. doi:10.1016/j.livsci.2014.10.005.

[13] Lucas D, Brun A, Gispert M, Carabús A, Soler J, Tibau J, et al. Relationship between pig carcass characteristics measured in live pigs or carcasses with Piglog, Fat-o-Meat'er and computed tomography. Livest Sci 2017;197:88–95. doi:10.1016/j.livsci.2017.01.010.

[14] Reynés B, van Schothorst EM, Keijer J, Palou A, Oliver P. Effects of cold exposure revealed by global transcriptomic analysis in ferret peripheral blood mononuclear cells. Sci Rep 2019;9:19985. doi:10.1038/s41598-019-56354-6.

[15] Zeng Y, David J, Rémond D, Dardevet D, Savary-Auzeloux I, Polakof S. Peripheral Blood Mononuclear Cell Metabolism Acutely Adapted to Postprandial Transition and Mainly Reflected Metabolic Adipose Tissue Adaptations to a High-Fat Diet in Minipigs. Nutrients 2018;10. doi:10.3390/nu10111816.

[16] Cifre M, Palou A, Oliver P. Cognitive impairment in metabolically-obese, normal-weight rats: identification of early biomarkers in peripheral blood mononuclear cells. Mol Neurodegener 2018;13:14. doi:10.1186/s13024-018-0246-8.
[17] Lelouvier B, Servant F, Païssé S, Brunet A-C, Benyahya S, Serino M, et al. Changes in blood microbiota profiles associated with liver fibrosis in obese patients: A pilot analysis. Hepatology 2016;64:2015–2027. doi:10.1002/hep.28829.
[18] Boada I, Spinola J, Rodriguez J, Martínez R. VisualPork towards the simulation of a virtual butcher. II Workshop on the Use Of … 2009.
[19] Bardera A, Martínez R, Boada I, Font-i-Furnols M. VisualPork towards the simulation of a virtual butcher. FAIM I Conference of COST … 2012.
[20] Serrano JCE, Gonzalo-Benito H, Jové M, Fourcade S, Cassanyé A, Boada J, et al. Dietary intake of green tea polyphenols regulates insulin sensitivity with an increase in AMP-activated protein kinase α content and changes in mitochondrial respiratory complexes. Mol Nutr Food Res 2013;57:459–470. doi:10.1002/mnfr.201200513.
[21] Hara A, Radin NS. Lipid extraction of tissues with a low-toxicity solvent. Anal Biochem 1978;90:420–426. doi:10.1016/0003-2697(78)90046-5.
[22] Pizarro C, Arenzana-Rámila I, Pérez-del-Notario N, Pérez-Matute P, González-Sáiz J-M. Plasma lipidomic profiling method based on ultrasound extraction and liquid chromatography mass spectrometry. Anal Chem 2013;85:12085–12092. doi:10.1021/ac403181c.
[23] Castro-Perez JM, Kamphorst J, DeGroot J, Lafeber F, Goshawk J, Yu K, et al. Comprehensive LC-MS E lipidomic analysis using a shotgun approach and its application to biomarker detection and identification in osteoarthritis patients. J Proteome Res 2010;9:2377–2389. doi:10.1021/pr901094j.
[24] Jové M, Moreno-Navarrete JM, Pamplona R, Ricart W, Portero-Otín M, Fernández-Real JM. Human omental and subcutaneous adipose tissue exhibit specific lipidomic signatures. FASEB J 2014;28:1071–1081. doi:10.1096/fj.13-234419.
[25] Sana TR, Roark JC, Li X, Waddell K, Fischer SM. Molecular formula and METLIN Personal Metabolite Database matching applied to the identification of compounds generated by LC/TOF-MS. J Biomol Tech 2008;19:258–266.
[26] Xia J, Sinelnikov IV, Han B, Wishart DS. MetaboAnalyst 3.0--making metabolomics more meaningful. Nucleic Acids Res 2015;43:W251–7. doi:10.1093/nar/gkv380.
[27] Kamburov A, Pentchev K, Galicka H, Wierling C, Lehrach H, Herwig R. ConsensusPathDB: toward a more complete picture of cell biology. Nucleic Acids Res 2011;39:D712–7. doi:10.1093/nar/gkq1156.
[28] Warde-Farley D, Donaldson SL, Comes O, Zuberi K, Badrawi R, Chao P, et al. The GeneMANIA prediction server: biological network integration for gene prioritization and predicting gene function. Nucleic Acids Res 2010;38:W214–20. doi:10.1093/nar/gkq537.
[29] White UA, Stephens JM. Transcriptional factors that promote formation of white adipose tissue. Mol Cell Endocrinol 2010;318:10–14. doi:10.1016/j.mce.2009.08.023.
[30] Spurlock ME, Gabler NK. The development of porcine models of obesity and the metabolic syndrome. J Nutr 2008;138:397–402. doi:10.1093/jn/138.2.397.
[31] Pawar AS, Zhu X-Y, Eirin A, Tang H, Jordan KL, Woollard JR, et al. Adipose tissue remodeling in a novel domestic porcine model of diet-induced obesity. Obesity (Silver Spring) 2015;23:399–407. doi:10.1002/oby.20971.
[32] Hill JO, Wyatt HR, Peters JC. Energy balance and obesity. Circulation 2012;126:126–132. doi:10.1161/CIRCULATIONAHA.111.087213.
[33] Steig AJ, Jackman MR, Giles ED, Higgins JA, Johnson GC, Mahan C, et al. Exercise reduces appetite and traffics excess nutrients away from energetically

efficient pathways of lipid deposition during the early stages of weight regain. Am J Physiol Regul Integr Comp Physiol 2011;301:R656–67. doi:10.1152/ajpregu.00212.2011.
[34] Zhang X, Lerman LO. The metabolic syndrome and chronic kidney disease. Transl Res 2017;183:14–25. doi:10.1016/j.trsl.2016.12.004.
[35] Galili O, Versari D, Sattler KJ, Olson ML, Mannheim D, McConnell JP, et al. Early experimental obesity is associated with coronary endothelial dysfunction and oxidative stress. Am J Physiol Heart Circ Physiol 2007;292:H904–11. doi:10.1152/ajpheart.00628.2006.
[36] Wu G, Zhang L, Li T, Zuniga A, Lopaschuk GD, Li L, et al. Choline supplementation promotes hepatic insulin resistance in phosphatidylethanolamine N-methyltransferase-deficient mice via increased glucagon action. J Biol Chem 2013;288:837–847. doi:10.1074/jbc.M112.415117.
[37] Jacobs RL, Zhao Y, Koonen DPY, Sletten T, Su B, Lingrell S, et al. Impaired de novo choline synthesis explains why phosphatidylethanolamine N-methyltransferase-deficient mice are protected from diet-induced obesity. J Biol Chem 2010;285:22403–22413. doi:10.1074/jbc.M110.108514.
[38] Holčapek M, Ovčačíková M, Lísa M, Cífková E, Hájek T. Continuous comprehensive two-dimensional liquid chromatography-electrospray ionization mass spectrometry of complex lipidomic samples. Anal Bioanal Chem 2015;407:5033–5043. doi:10.1007/s00216-015-8528-2.
[39] Meikle PJ, Wong G, Barlow CK, Weir JM, Greeve MA, MacIntosh GL, et al. Plasma lipid profiling shows similar associations with prediabetes and type 2 diabetes. PLoS One 2013;8:e74341. doi:10.1371/journal.pone.0074341.
[40] Wallace M, Morris C, O'Grada CM, Ryan M, Dillon ET, Coleman E, et al. Relationship between the lipidome, inflammatory markers and insulin resistance. Mol Biosyst 2014;10:1586–1595. doi:10.1039/c3mb70529c.
[41] Heilbronn LK, Coster ACF, Campbell LV, Greenfield JR, Lange K, Christopher MJ, et al. The effect of short-term overfeeding on serum lipids in healthy humans. Obesity (Silver Spring) 2013;21:E649–59. doi:10.1002/oby.20508.
[42] Douglass JD, Zhou YX, Wu A, Zadrogra JA, Gajda AM, Lackey AI, et al. Global deletion of MGL in mice delays lipid absorption and alters energy homeostasis and diet-induced obesity. J Lipid Res 2015;56:1153–1171. doi:10.1194/jlr.M058586.
[43] Wu X-F, Wu X-X, Guo W-J, Luo Q, Gu Y-H, Shen Y, et al. Cerebroside D, a glycoceramide compound, improves experimental colitis in mice with multiple targets against activated T lymphocytes. Toxicol Appl Pharmacol 2012;263:296–302. doi:10.1016/j.taap.2012.07.001.
[44] Margalit M, Shalev Z, Pappo O, Sklair-Levy M, Alper R, Gomori M, et al. Glucocerebroside ameliorates the metabolic syndrome in OB/OB mice. J Pharmacol Exp Ther 2006;319:105–110. doi:10.1124/jpet.106.104950.
[45] Chavez JA, Summers SA. A ceramide-centric view of insulin resistance. Cell Metab 2012;15:585–594. doi:10.1016/j.cmet.2012.04.002.
[46] Eisinger K, Liebisch G, Schmitz G, Aslanidis C, Krautbauer S, Buechler C. Lipidomic analysis of serum from high fat diet induced obese mice. Int J Mol Sci 2014;15:2991–3002. doi:10.3390/ijms15022991.
[47] Weir JM, Wong G, Barlow CK, Greeve MA, Kowalczyk A, Almasy L, et al. Plasma lipid profiling in a large population-based cohort. J Lipid Res 2013;54:2898–2908. doi:10.1194/jlr.P035808.
[48] Korkes HA, Sass N, Moron AF, Câmara NOS, Bonetti T, Cerdeira AS, et al. Lipidomic assessment of plasma and placenta of women with early-onset preeclampsia. PLoS One 2014;9:e110747. doi:10.1371/journal.pone.0110747.
[49] Leventis PA, Grinstein S. The distribution and function of phosphatidylserine in cellular membranes. Annu Rev Biophys 2010;39:407–427. doi:10.1146/annurev.biophys.093008.131234.

[50] Grace MS, Dempsey PC, Sethi P, Mundra PA, Mellett NA, Weir JM, et al. Breaking up prolonged sitting alters the postprandial plasma lipidomic profile of adults with type 2 diabetes. J Clin Endocrinol Metab 2017;102:1991–1999. doi:10.1210/jc.2016-3926.
[51] Sanyal AJ, Pacana T. A Lipidomic Readout of Disease Progression in A Diet-Induced Mouse Model of Nonalcoholic Fatty Liver Disease. Trans Am Clin Climatol Assoc 2015;126:271–288.
[52] Gorden DL, Myers DS, Ivanova PT, Fahy E, Maurya MR, Gupta S, et al. Biomarkers of NAFLD progression: a lipidomics approach to an epidemic. J Lipid Res 2015;56:722–736. doi:10.1194/jlr.P056002.
[53] Aburasayn H, Al Batran R, Ussher JR. Targeting ceramide metabolism in obesity. Am J Physiol Endocrinol Metab 2016;311:E423–35. doi:10.1152/ajpendo.00133.2016.
[54] Giesbertz P, Daniel H. Branched-chain amino acids as biomarkers in diabetes. Curr Opin Clin Nutr Metab Care 2016;19:48–54. doi:10.1097/MCO.0000000000000235.
[55] Polakof S, Dardevet D, Lyan B, Mosoni L, Gatineau E, Martin J-F, et al. Time Course of Molecular and Metabolic Events in the Development of Insulin Resistance in Fructose-Fed Rats. J Proteome Res 2016;15:1862–1874. doi:10.1021/acs.jproteome.6b00043.
[56] Zhang J, Zhang Y, Sun T, Guo F, Huang S, Chandalia M, et al. Dietary obesity-induced Egr-1 in adipocytes facilitates energy storage via suppression of FOXC2. Sci Rep 2013;3:1476. doi:10.1038/srep01476.
[57] Aljada A, Ghanim H, Mohanty P, Kapur N, Dandona P. Insulin inhibits the pro-inflammatory transcription factor early growth response gene-1 (Egr)-1 expression in mononuclear cells (MNC) and reduces plasma tissue factor (TF) and plasminogen activator inhibitor-1 (PAI-1) concentrations. J Clin Endocrinol Metab 2002;87:1419–1422. doi:10.1210/jcem.87.3.8462.
[58] Giannini C, Feldstein AE, Santoro N, Kim G, Kursawe R, Pierpont B, et al. Circulating levels of FGF-21 in obese youth: associations with liver fat content and markers of liver damage. J Clin Endocrinol Metab 2013;98:2993–3000. doi:10.1210/jc.2013-1250.
[59] Liu P, Hsieh P, Lin H, Liu T, Wu H, Chen C, et al. Grail is involved in adipocyte differentiation and diet-induced obesity. Cell Death Dis 2018;9:525. doi:10.1038/s41419-018-0596-8.
[60] Son MJ, Kim WK, Oh K-J, Park A, Lee DS, Han BS, et al. Methyltransferase and demethylase profiling studies during brown adipocyte differentiation. BMB Rep 2016;49:388–393. doi:10.5483/BMBRep.2016.49.7.062.
[61] Wright TM, King MV, Davey WG, Langley-Evans SC, Voigt J-PW. Impact of cafeteria feeding during lactation in the rat on novel object discrimination in the offspring. Br J Nutr 2014;112:1–5. doi:10.1017/S0007114514003134.
[62] Krawczyńska A, Herman AP, Antushevich H, Bochenek J, Dziendzikowska K, Gajewska A, et al. Modifications of Western-type diet regarding protein, fat and sucrose levels as modulators of steroid metabolism and activity in liver. J Steroid Biochem Mol Biol 2017;165:331–341. doi:10.1016/j.jsbmb.2016.07.012.
[63] Sari G, Meester EJ, van der Zee LC, Wouters K, van Lennep JR, Peppelenbosch M, et al. A mouse model of humanized liver shows a human-like lipid profile, but does not form atherosclerotic plaque after western type diet. Biochem Biophys Res Commun 2020. doi:10.1016/j.bbrc.2020.01.067.
[64] Statovci D, Aguilera M, MacSharry J, Melgar S. The impact of western diet and nutrients on the microbiota and immune response at mucosal interfaces. Front Immunol 2017;8:838. doi:10.3389/fimmu.2017.00838.
[65] Sumner LW, Amberg A, Barrett D, Beale MH, Beger R, Daykin CA, et al. Proposed minimum reporting standards for chemical analysis Chemical Analysis

Working Group (CAWG) Metabolomics Standards Initiative (MSI). Metabolomics 2007;3:211–221. doi:10.1007/s11306-007-0082-2.

[66] Vukovic R, Dos Santos TJ, Ybarra M, Atar M. Children with metabolically healthy obesity: A review. Front Endocrinol (Lausanne) 2019;10:865. doi:10.3389/fendo.2019.00865.

FIGURE LEGENDS

Figure 1. **A western-type diet induces prepubertal obesity, and it defines a specific lipidomic signature in plasma**. A) Representative CT images of the porcine model of prepuberal obesity showing accumulation of AT in animals under a western-type diet. B) Example of determination of subcutaneous fat (red), intermuscular fat (green), and flare fat, including pelvic-renal depot (orange) from CT images. C) Hierarchical clustering and heatmap shows a plasma lipidomic signature of high-calorie (western-type diet) in the porcine model. In the right panel, the PLS-DA model using plasma lipidomics demonstrates high accuracy (>65%, R^2=0.99) in classification. Selected lipids are significantly associated with individual calorie intake (D), global fat abundance (E), and pelvic-rrenal fat abundance (F) as measured by CT in vivo. Shown lipids are a selection from those showing a significant correlation with specific traits (at least $p<0.05$ by Spearman's rank correlation test, lines indicate non-linear fit (exponential growth equations; Y=Y0*exp(k*X)). see Supplemental Data for the whole list).

Figure 2. The prepubescent obesity model described induces changes in circulating insulin levels and its action, in association with specific plasma lipids and with changes in AT insulin-regulated proteins. Association of plasma concentration of selected lipids with individual insulin concentrations and HOMA-IR values (A). B shows a representative western-blot of insulin-responsive signals in AT and the influence of western-type diet. Right graphs after each blot show densitometric integrated values normalized to the intensity of animals fed with conventional diets all adjusted to total protein content, estimated by Coomassie blue staining, with p values after Students t-test. Considering all values from each protein, with a two way ANOVA significant differences were found as well for Glut2 in the subcutaneous depot, and for SREBP1 in omental and pelvic-renal depots ($p<0.05$, $p<0.01$ and $p<0.02$ respectively by post hoc analyses, n ranging 3 to 9 different samples). C) Subcutaneous adipose tissue leptin mRNA levels are associated with specific circulating lipids. D) Venn diagram showing the specificity of correlations, based on the very low (or absent) overlap between circulating lipids associated (at least $p<0.05$ by Spearman's rank correlation test) with HOMA-IR, with subcutaneous adipose tissue leptin mRNA, and with fat content. Shown lipids in A and C are a selection from those showing significant correlation with these specific traits (at least $p<0.05$ by Spearman's rank

819 correlation test, lines indicate non-linear fit (exponential growth equations; Y=Y0*exp(k*X), see
820 Supplemental Data for the whole list)
821
822 Figure 3. **Liver insulin-responsive signals and relationship with circulating lipidome**. A)
823 Representative western-blot of insulin-responsive signals in the liver with * in Glut 2 indicating
824 differences induced by western-type diet ($p<0.05$ by Student's t-test). B) Liver triacylglyceride
825 (TAG) levels are associated with specific circulating lipids. C) Venn diagram showing the
826 specificity of correlations, based on the very low (or absent) overlap between circulating lipids
827 associated (at least $p<0.05$ by Spearman's rank correlation test) with hepatic TAG levels, with
828 HOMA-IR, with subcutaneous adipose tissue leptin mRNA and with fat content. Shown lipids in
829 B are a selection from those showing significant correlation with specific traits (at least $p<0.05$ by
830 Spearman's rank correlation test, lines indicate non-linear fit (exponential growth equations;
831 Y=Y0*exp(k*X)), see Supplemental Data for the whole list)
832
833 Figure 4. **Validation in humans with obesity of proposed biomarkers.** Specific lipids show a
834 similar positive correlation with BMI (in humans, in B, D, and F) and AT abundance (in the porcine
835 model, in A, C, and E). The same is presented for HOMA-IR correlations (for pigs in G and
836 humans in H). All correlations are significant (at least $p<0.05$) by Spearman's rank correlation
837 test. Lines indicate non-linear fit (exponential growth equations; Y=Y0*exp(k*X)). Pig icon comes
838 from aLf; and Human one by Ma Qing both from the Noun Project (thenountproject.com)
839
840 Figure 5. **Interactomics of plasma metabolites associated with a western-type diet**.
841 Metabolites were mapped to a pathway database (in this case, KEGG), and nodes, representing
842 pathways (identified by pathway name in the database), is proportional to the number of
843 metabolites contained in the pathway. Node color intensity is associated with the hypergeometric
844 test accounting number of metabolites associated with high-calorie diet and those potentially
845 present in the specific pathway (node), while edge width represents the percentage of shared
846 metabolites between pathways and edge color indicate the number of metabolites associated
847 with western-type diet.
848

Table 1. Morphological, calorie consumption and biochemical traits

Parameter	Conventional diet	Western-type diet	p[1]
Initial weight (Kg)	16.5±2.8	16.7±2.2	0.86
Final weight (Kg)	53.2±5.7	60±8.36	0.043
Weight gain (Kg/d)	0.58±0.06	0.68±0.1	0.024
Caloric consumption (Kcal/d)	3819.7±236.5	5213.9±516.8	<0.0001
Fecal fat content (mg/g)	19.5±1.3	50±8	0.02
Pelvico-renal fat weight (Kg)	0.188±0.026	0.405±0.082	0.008
Relative fat volume at VL2 (%)	12.7±1.2	19.4±2.6	0.002
Blood Cholesterol (mg/dL)	125.9±24.4	155.7±26.4	0.015
Blood LDL-Cholesterol (mg/dL)	46.8±8.1	57.1±8.5	0.011
Blood HDL-Cholesterol (mg/dL)	45.2±9.9	61.3±13.8	0.007
Triacylglyceridemia (mg/dL)	21.6±6.3	29.2±5.9	0.014
Glycemia (mg/dL)	80.75±16.73	108.6±23.9	0.01
Fructosamine (mg/dL)	177.6±24.9	152.1±46.8	0.131
Insulinemia (pg/mL)	5.65±0.24	5.77±0.46	0.26
HOMA-IR	1.09±0.21	1.56±0.39	0.009

Values shown are mean±SD, unless stated otherwise. [1]Student's t test comparison between values in in conventional and western-type diets

FIGURE 1

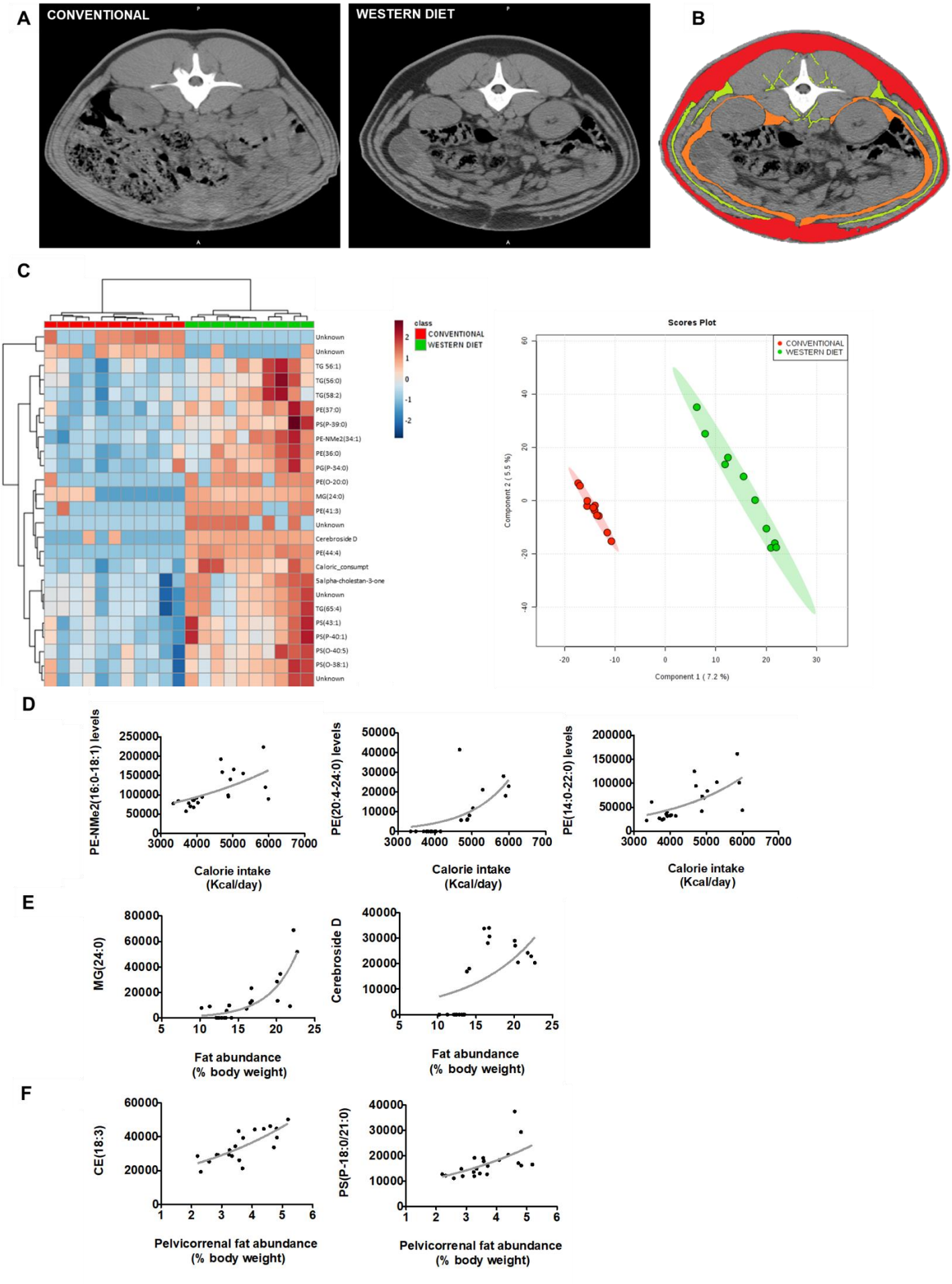
A
CONVENTIONAL
WESTERN DIET
B
C
class
CONVENTIONAL
WESTERN DIET
Unknown
Unknown
TG 56:1)
TG(56:0)
TG(58:2)
PE(37:0)
PS(P-39:0)
PE-NMe2(34:1)
PE(36:0)
PG(P-34:0)
PE(O-20:0)
MG(24:0)
PE(41:3)
Unknown
Cerebroside D
PE(44:4)
Caloric_consumpt
Salpha-cholestan-3-one
Unknown
TG(65:4)
PS(43:1)
PS(P-40:1)
PS(O-40:5)
PS(O-38:1)
Unknown
Scores Plot
CONVENTIONAL
WESTERN DIET
Component 2 (5.5 %)
Component 1 (7.2 %)
D
PE-NMe2(16:0-18:1) levels
Calorie intake (Kcal/day)
PE(20:4-24:0) levels
Calorie intake (Kcal/day)
PE(14:0-22:0) levels
Calorie intake (Kcal/day)
E
MG(24:0)
Fat abundance (% body weight)
Cerebroside D
Fat abundance (% body weight)
F
CE(18:3)
Pelvicorrenal fat abundance (% body weight)
PS(P-18:0/21:0)
Pelvicorrenal fat abundance (% body weight)

FIGURE 2

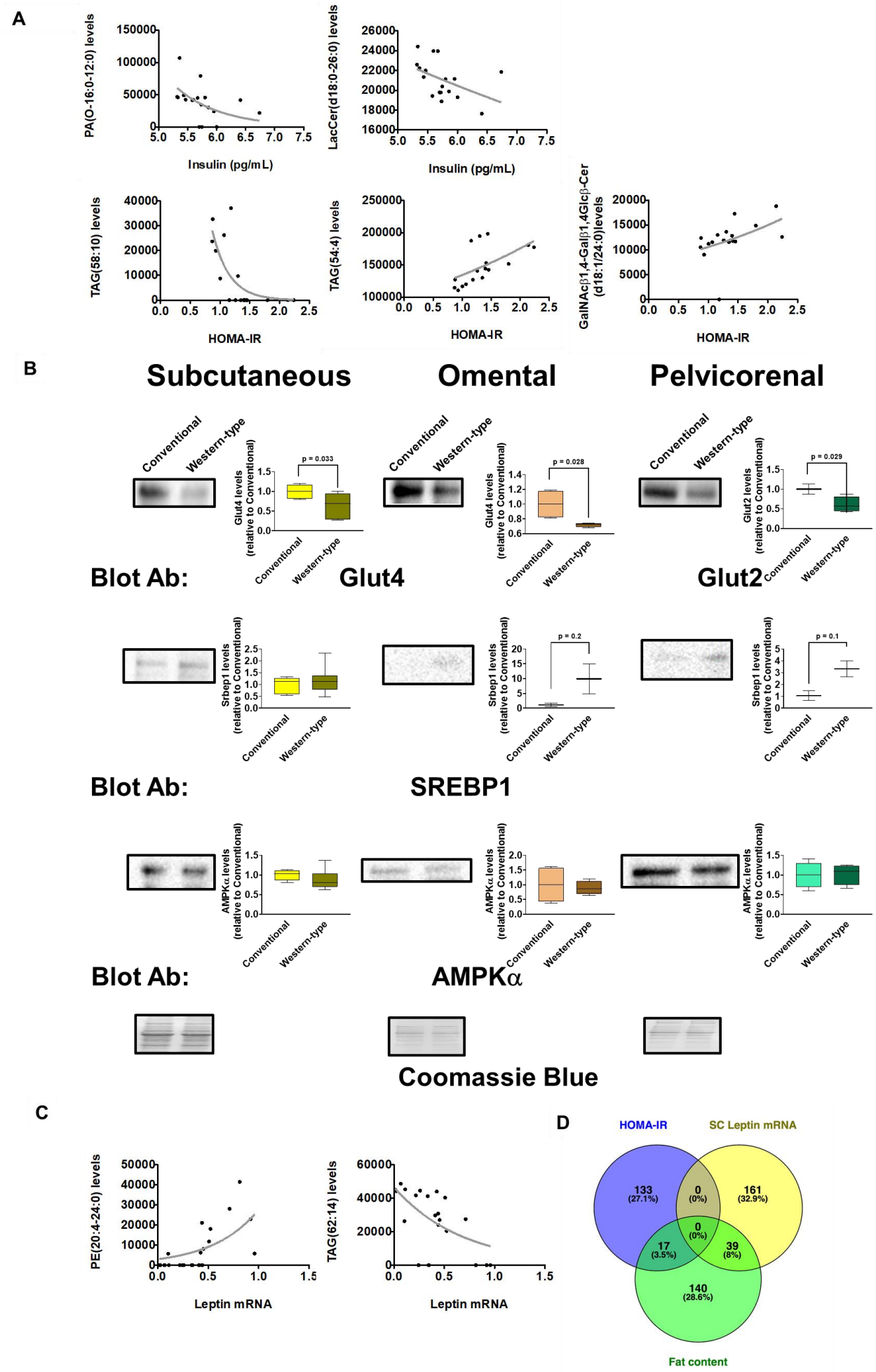
A
PA(O-16:0-12:0) levels
Insulin (pg/mL)
LacCer(d18:0-26:0) levels
Insulin (pg/mL)
TAG(58:10) levels
HOMA-IR
TAG(54:4) levels
HOMA-IR
GalNAcβ1,4-Galβ1,4Glcβ-Cer (d18:1/24:0)levels
HOMA-IR
B
Subcutaneous
Omental
Pelvicorenal
Conventional
Western-type
p = 0.033
p = 0.028
p = 0.029
Glut4 levels (relative to Conventional)
Glut2 levels (relative to Conventional)
Blot Ab:
Glut4
Glut2
p = 0.2
p = 0.1
Srbep1 levels (relative to Conventional)
Blot Ab:
SREBP1
AMPKα levels (relative to Conventional)
Blot Ab:
AMPKα
Coomassie Blue
C
PE(20:4-24:0) levels
Leptin mRNA
TAG(62:14) levels
Leptin mRNA
D
HOMA-IR
SC Leptin mRNA
Fat content
133 (27.1%)
0 (0%)
161 (32.9%)
0 (0%)
17 (3.5%)
39 (8%)
140 (28.6%)

FIGURE 3

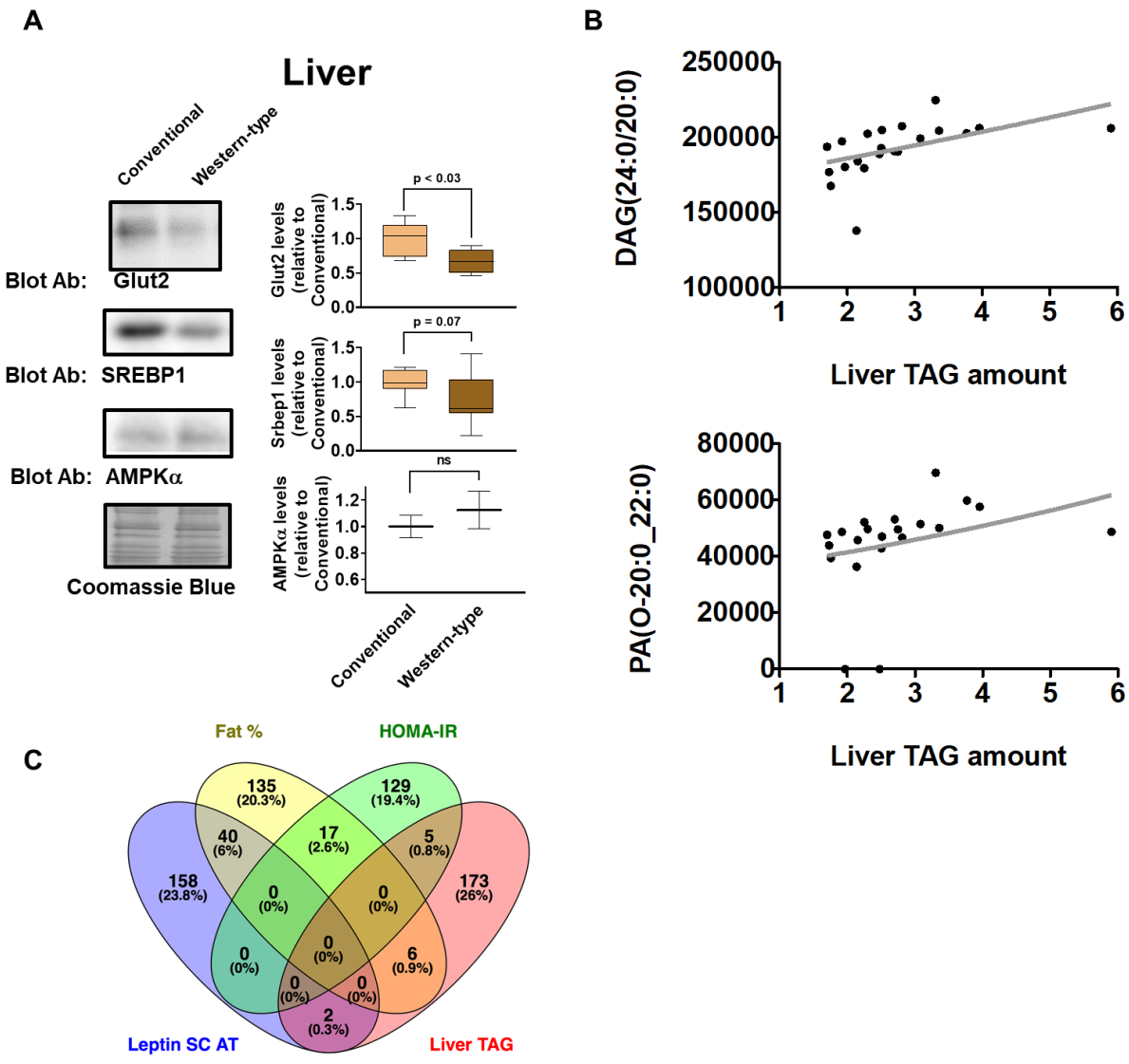
A
Liver
Conventional
Western-type
Blot Ab: Glut2
Blot Ab: SREBP1
Blot Ab: AMPKα
Coomassie Blue
Glut2 levels (relative to Conventional)
p < 0.03
Srbep1 levels (relative to Conventional)
p = 0.07
AMPKα levels (relative to Conventional)
ns
Conventional
Western-type
B
DAG(24:0/20:0)
Liver TAG amount
PA(O-20:0_22:0)
Liver TAG amount
C
Fat %
HOMA-IR
Leptin SC AT
Liver TAG
135 (20.3%)
129 (19.4%)
40 (6%)
17 (2.6%)
5 (0.8%)
158 (23.8%)
173 (26%)
0 (0%)
0 (0%)
0 (0%)
0 (0%)
6 (0.9%)
0 (0%)
0 (0%)
2 (0.3%)

FIGURE 4

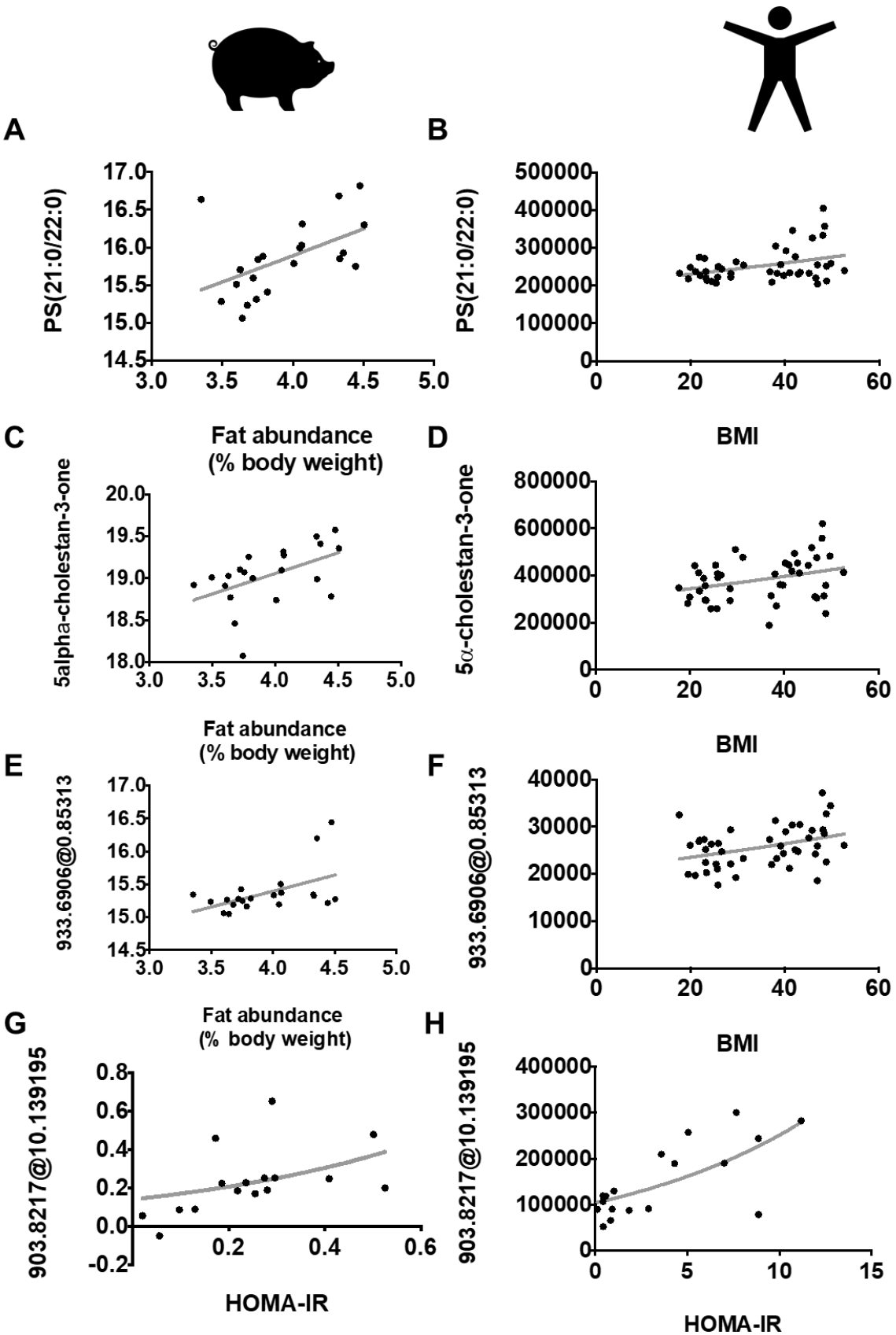
A
B
PS(21:0/22:0)
17.0
16.5
16.0
15.5
15.0
14.5
3.0
3.5
4.0
4.5
5.0
500000
400000
300000
200000
100000
0
0
20
40
60
C
D
Fat abundance
(% body weight)
BMI
5alpha-cholestan-3-one
5α-cholestan-3-one
20.0
19.5
19.0
18.5
18.0
800000
600000
400000
200000
E
F
933.6906@0.85313
40000
30000
20000
10000
G
H
903.8217@10.139195
0.8
0.6
0.4
0.2
0.0
-0.2
0.2
0.4
0.6
HOMA-IR
400000
300000
200000
100000
0
5
10
15

FIGURE 5

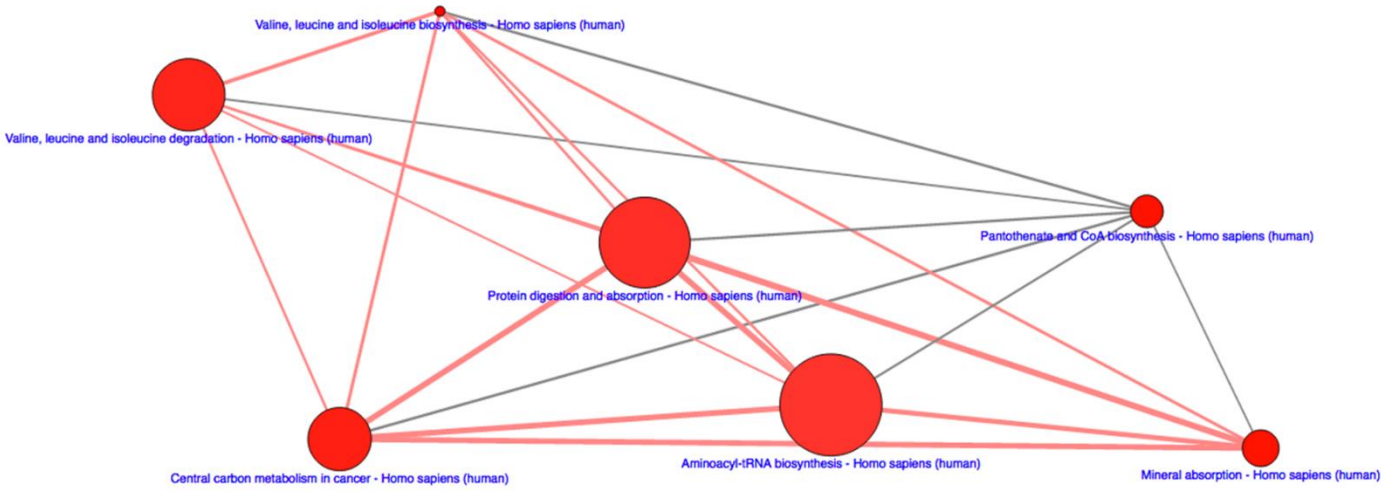
Valine, leucine and isoleucine biosynthesis - Homo sapiens (human)
Valine, leucine and isoleucine degradation - Homo sapiens (human)
Pantothenate and CoA biosynthesis - Homo sapiens (human)
Protein digestion and absorption - Homo sapiens (human)
Aminoacyl-tRNA biosynthesis - Homo sapiens (human)
Central carbon metabolism in cancer - Homo sapiens (human)
Mineral absorption - Homo sapiens (human)

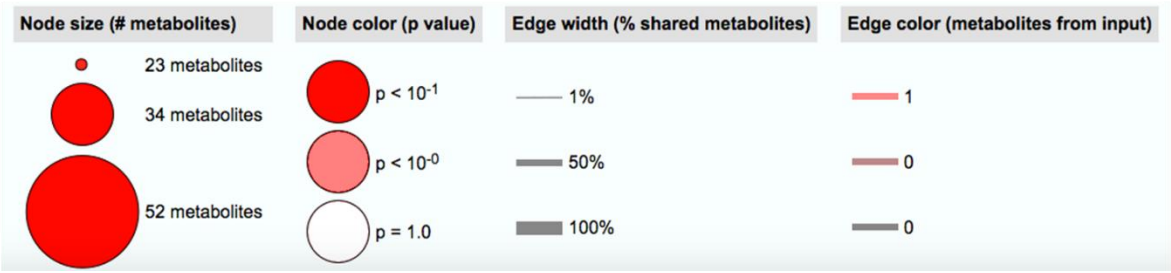
Node size (# metabolites)
23 metabolites
34 metabolites
52 metabolites
Node color (p value)
p < 10-1
p < 10-0
p = 1.0
Edge width (% shared metabolites)
1%
50%
100%
Edge color (metabolites from input)
1
0
0

EXTENDED METHODS

Chemicals

For lipidomic analyses and other analytical procedures, synthetic lipids were obtained from Avanti Polar Lipids Inc. (Alabaster, AL, USA) and Sigma-Aldrich (Madrid, Spain). Methyl tert-butyl ether (MTBE), acetonitrile, potassium chloride, chloroform, ammonium formate and ammonium hydroxide -all liquid chromatography-mass spectrometry (LC-MS) grade- were purchased from Sigma-Aldrich (Madrid, Spain); methanol was from Carlo Erba (Milano, Italy); acetone was from Riedel-de-Häen (Seelze, Germany); and LC/MS-grade isopropanol and formic acid were from Baker (Phillipsburg, NJ, USA).

Computed tomography scanning and image analysis

Previously to the scan, animals were fasted for 16 h and anesthetized with azaperone (0.1 mg/kg body weight (BW)), ketamine (0.2 mg/kg BW), and, if necessary, propofol (0.22 mg/kg BW) as explained in [1]. Pigs were scanned in the prone position, and acquisition parameters were axial, 1 s, 140 kV, 145 mA, 5 mm thickness, matrix 512x512, and displayed field of view adapted to the size of each pig. Scanning lasted approximately 20 min per pig. For each pig, one axial image was obtained at the level of the 2nd lumbar vertebrae (2VL).

Images were analyzed with the software VisualPork [2,3] developed by the University of Girona and IRTA. Image analysis was those explained in ValLaillet *et al.* [4] modified. Thus, the mean and standard deviation of the Hounsfield (HU) value of the subcutaneous fat were obtained from each image. These values were used for the determination of the fat tissue content. From each image, an ROI (region of interest) was determined that considered all the outlines of the pig (ROI1), *i.e.,* the total area of the image. Another area was taken at for the interior part of the subcutaneous fat of each image (ROI2), which corresponds to the area of the image, excluding subcutaneous fat and skin. Another area was obtained, including all the intraabdominal region, being the ribs, and the tenderloin the borders (ROI3). Finally, intraperitoneal area, going through the junction between flare fat and internal organs (ROI4),

was determined. For each ROI (from ROI1 to ROI4), the AT area was calculated, considering the range of HU values between the mean HU value plus/minus two standard deviations previously determined. These areas were transformed into $mm^{3,}$ considering the DFOV, the matrix size, and the thickness [5]. From the volume of ROI1 minus those from ROI2, the subcutaneous fat was obtained. Intermuscular fat was obtained as the fat volume in ROI2 minus ROI3 and flare fat as the fat volume of ROI3 minus those of ROI4. The ratio between the volume of the total fat (subcutaneous, intermuscular, and flare fat) and the total volume of the image was determined and converted into a percentage (relative fat volume at VL2).

Samples were homogenized in a buffer containing 180 mM KCl, five mM MOPS, two mM EDTA, one mM diethylenetriaminepentaacetic acid, and one μM butylated hydroxyl toluene, 10 μg/ml aprotinin, one mM NaF, one mM Na3VO4 and a protease inhibitor mix (GE Healthcare 80-6501-23, USA) (1% v/v) with a Potter-Elvehjem device, at 4 °C. After brief centrifugation (500 × g, 5 min) protein concentrations were measured in the supernatants using the Bradford protein assay (BioRad Laboratories, München, Germany). Tissue protein (15-40 mg) was resolved by SDS-PAGE and electroblotted onto polyvinylidene difluoride membranes (Immobilon-P, Millipore, Bedford, USA). Immunodetection was performed using as primary and secondary antibodies, those listed in Supplemental Table 6. A monoclonal antibody to β-actin (Sigma, USA) and Coomassie blue staining were used to control protein loading. Protein bands were visualized with the chemiluminescence ECL method (Millipore Corporation, Billerica, MA, USA). Luminescence was recorded and quantified in Lumi-Imager equipment from Boehringer (Mannheim, Germany), using the Quantity One 4.6.5. Software.

Lipidomic analyses

Preparation of Lipid Standards Lipid standards consisting of isotopically labeled lipids (see Supplemental Table 7) were used for external standardization (i.e., lipid family assignment) and internal standardization (i.e., for adjustment of potential inter- and intra-assay variances). Stock solutions were prepared by dissolving lipid standards in MTBE at a concentration of 1mg/mL, and working solutions were diluted to 2.5μg/mL in MTBE.

Lipid extraction Briefly, in order to precipitate plasma protein fraction, 5µl of Mili Q water and 20µl of methanol were added to 10µl of a plasma sample. After the addition, samples were vigorously shaken for 2 min. Then, for lipid extraction, 250µl of MTBE (containing internal lipid standards) were added, and samples were immersed in a water bath (ATU Ultrasonidos, Valencia, Spain) with an ultrasound frequency and power of 40kHz and 100W, respectively, at 10°C for 30 min. Then, 75 µL of Mili Q water was added to the mixture, and the organic phase was separated by centrifugation (1,400 x g) at 10 °C for 10 min. Lipid extracts contained in the upper phase were collected and subjected to mass spectrometry. A pool of all lipid extracts was prepared and used as quality controls, as previously described [6].

LC-MS/MS method Sample compartment was refrigerated at 4°C, and for each sample, 10µl of lipid extract was applied onto 1.8 µm particle 100 x 2.1 mm id Waters Acquity HSS T3 column (Waters, Milford, MA, USA) heated to 55°C. The flow rate was 400µl/min with solvent A composed of 10mM ammonium acetate in acetonitrile-water (40:60, v/v) and solvent B composed of 10mM ammonium acetate in acetonitrile-isopropanol (10:90, v/v). The gradient started at 40% B and reached 100% B in 10min and held for 2 min. Finally, the system was switched back to 60% B and equilibrated for 3min. Duplicate runs of the samples were performed to collect positive and negative electrospray ionized lipid species in a TOF mode, operated in full-scan mode at 100 to 3000m/z in an extended dynamic range (2 GHz), using N_2 as nebulizer gas (5L/min, 350°C). The capillary voltage was set 3500 V with a scan rate of 1scan/s. Continuous infusion using a double spray with masses 121.050873, 922.009798 (positive ion mode), and 119.036320, 966.000725 (negative ion mode) was used for in-run calibration of the mass spectrometer.

Untargeted metabolomics analyses of serum

For extraction of metabolites, 1.8ml of a methanol/water 8:1 (v/v) was added to 200 µl of serum sample. After stirring for 1 min and centrifugation (1400 x g) for 10 min at 4ºC, the supernatant with water-soluble metabolites was placed into a new vial, and the pellet was washed twice

with additional methanol/water. The combined upper-phases solutions were partially dried under N_2 flow until methanol removal. Finally, the solution was quickly frozen and lyophilized.

The LC-MS analysis of aqueous serum extract samples was done using a Q-TOF/MS 6550 mass spectrometer (Agilent Technologies) with an Agilent UPLC 1290 chromatographic system. The lyophilized samples were reconstituted by adding 200 µl of 0.1% formic acid in water and injected onto a 1.8 µm particle 50 x 2.1 mm id Zorbax SB-Aq RR column (Agilent Technologies) which was heated to 60ºC in the column oven. A binary gradient system consisting of 0.2% acetic acid in water (solvent A) and 0.2% acetic acid in methanol (solvent B) was used. The flow rate was 0.5 mL/min, and the solvent gradient program was 0 to 1 min 2% B isocratic, 1 to 13 min 98% B, 13 to 19 min 98% B isocratic, 1 min 0% B, and then equilibrated for an additional 5 min. The autosampler temperature was maintained at 4ºC, and the injection volume was 10 µl.

Ionization was performed in an electrospray source mode, with a drying gas temperature and a flow of 150ºC and 14 mL/min, respectively; a sheath gas temperature and flow of 300ºC and 11 mL/min, respectively; a nebulizer pressure of 30 psi; a capillary voltage of 3,000 V; and a nozzle voltage of 500 V. QTOF was operated in MS Full Scan mode in positive polarity, applying a fragmentary voltage of 380 V, an acquisition rate of 5 spectra/s and an acquisition range from 50 to 1700 m/z. Blank samples and quality control samples were injected regularly between the runs to ensure the quality of the data.

Peripheral blood monocyte cells (PBMC) and AT transcriptomics

Briefly, PBMCs were isolated from animal blood by Ficoll gradient separation (GE Healthcare, Piscataway, NJ, USA) and PBMC total RNA was extracted using Tripure Reagent (Roche Diagnostic, Barcelona, Spain) and purified with Qiagen RNeasy Mini Kit spin columns (Izasa, Barcelona, Spain). Blood samples (10 mL) were diluted (1:1) with phosphate buffer saline (pH: 7.4), and PBMC were isolated by Ficoll gradient separation, according to the instructions indicated by the manufacturer (GE Healthcare Bio Sciences). The PBMC pellet was carefully

resuspended with 4 mL of erythrocyte lysis buffer (155 mM NH_4Cl, ten mM $KHCO_3$, and 100 µM EDTA, pH: 7.4), incubated at room temperature for 5 minutes and centrifuged at 400 g for 10 minutes. Finally, the supernatant was aspirated, and the PBMC pellet was stored at -70°C until RNA analysis. PBMC total RNA was extracted using Tripure Reagent (Roche Diagnostic) and purified with Qiagen RNeasy Mini Kit spin columns (Izasa). RNA quantity was measured spectrophotometrically (NanoDrop®), and RNA quality was confirmed with the Agilent 2100 Bioanalyzer (Agilent Technologies).

The gene expression levels were assessed using Porcine (V2) Gene Expression Microarray, 4x44K (Agilent Technologies) following the manufacturer's instructions. This microarray quantifies 43,603 probe sets. Labeling and hybridization of the samples were performed following Agilent One-color Microarray-Based Gene Expression Analysis-Low Input Quick Amp Labelling kit v6.6 protocol. Arrays were scanned with a G2565A Microarray Scanner System with SureScan High-Resolution Technology, and spot intensities were quantified using Feature Extraction 11.5.1.1 (Agilent Technologies, Inc. Santa Clara, CA). Background correction and inter-array normalization were performed with GeneSpring software v12.6.1 (Agilent Technologies). Gene expression summaries were created for each gene by averaging all probe sets for each gene. All data analysis was conducted on gene-summarized data. Processed data were subsequently filtered for significant detection (P-value ≤ 0.01).

Quantitative analyses of selected mRNA in subcutaneous AT was performed as previously described [7]. Briefly, RNA was prepared from tissue samples using an RNeasy Lipid Tissue Mini Kit (Izasa). The integrity of each RNA sample was checked by an Agilent Bioanalyzer (Agilent Technologies). Total RNA was quantified by the use of a spectrophotometer (GeneQuant; GE Healthcare) and reverse transcribed to cDNA using a High Capacity cDNA Archive Kit (Applied Biosystems Inc., Madrid, Spain) according to the manufacturer's protocol. Gene expression was assessed by real-time PCR using a LightCycler 480 Real-Time PCR

System (Roche Diagnostics) using TaqMan® technology suitable for relative gene expression quantification.

REFERENCES

[1] Carabús A, Gispert M, Brun A, Rodríguez P, Font-i-Furnols M. In vivo computed tomography evaluation of the composition of the carcass and main cuts of growing pigs of three commercial crossbreeds. Livest Sci 2014;170:181–192. DOI:10.1016/j.livsci.2014.10.005.

[2] Boada I, Spinola J, Rodriguez J, Martínez R. VisualPork towards the simulation of a virtual butcher. II Workshop on the Use Of … 2009.

[3] Bardera A, Martínez R, Boada I, Font-i-Furnols M. VisualPork towards the simulation of a virtual butcher. FAIM I Conference of COST … 2012.

[4] Val-Laillet D, Blat S, Louveau I, Malbert CH. A computed tomography scan application to evaluate adiposity in a minipig model of human obesity. Br J Nutr 2010;104:1719–1728. DOI:10.1017/S0007114510002667.

[5] Furnols MF I, Teran MF, Gispert M. Estimation of lean meat content in pig carcasses using X-ray computed tomography and PLS regression. … and Intelligent Laboratory … 2009.

[6] Want EJ, Masson P, Michopoulos F, Wilson ID, Theodoridis G, Plumb RS, et al. Global metabolic profiling of animal and human tissues via UPLC-MS. Nat Protoc 2013;8:17–32. DOI:10.1038/nprot.2012.135.

[7] Jové M, Moreno-Navarrete JM, Pamplona R, Ricart W, Portero-Otín M, Fernández-Real JM. Human omental and subcutaneous adipose tissue exhibit specific lipidomic signatures. FASEB J 2014;28:1071–1081. DOI:10.1096/fj.13-234419.

Supplemental Figure 1

A

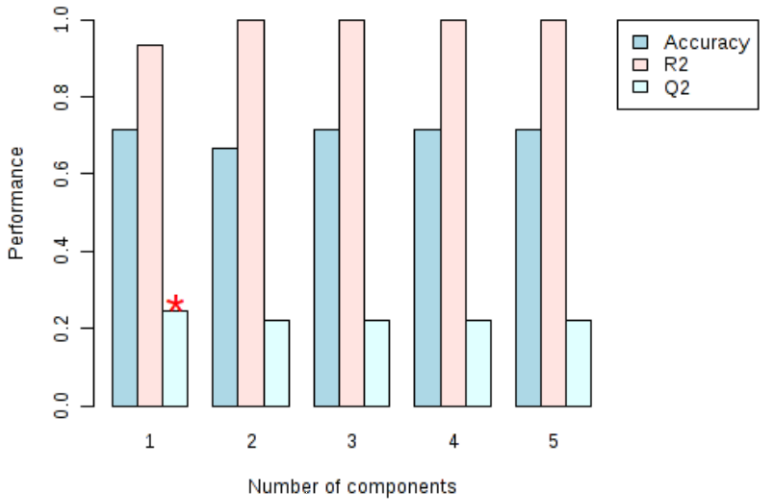

Measure	1 comps	2 comps	3 comps	4 comps	5 comps
Accuracy	0.71429	0.66667	0.71429	0.71429	0.71429
R2	0.93186	0.99808	0.99989	1.0	1.0
Q2	0.24573	0.22273	0.22017	0.2211	0.22109

B

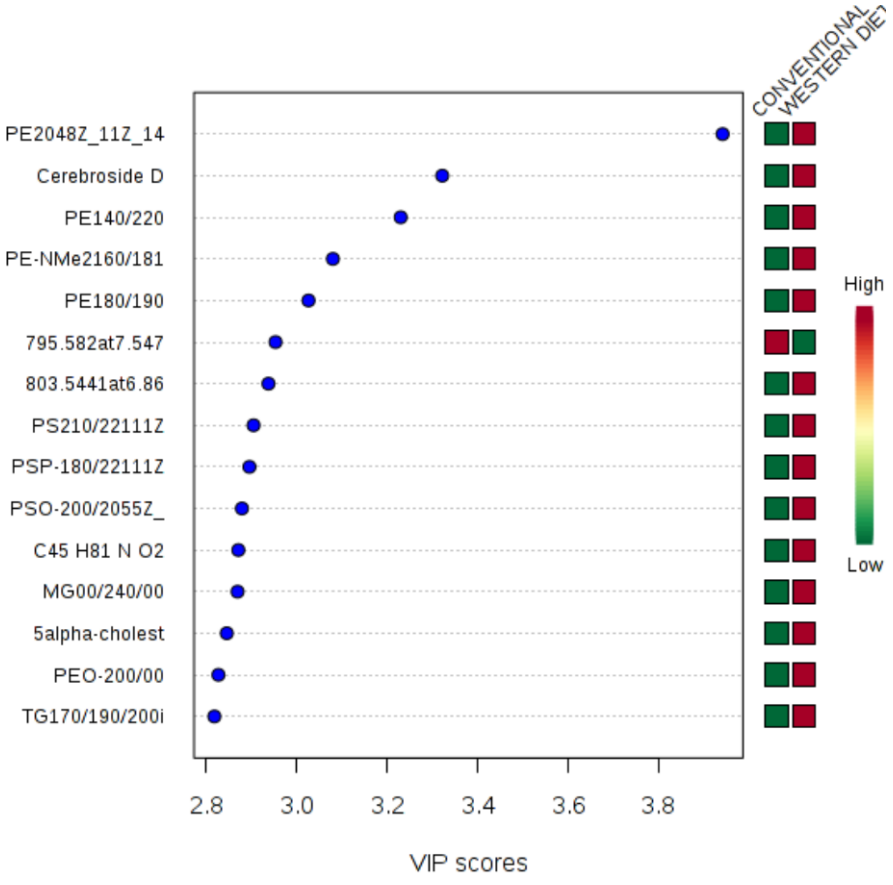

Supplemental Figure 1. Robustness of the PLS-DA model defining changes induced by a western-type diet (Figure 1 in the main text) is ensured by high accuracy, R2, and Q2 values. Variable importance in the projection of the first component demonstrates the importance of specific lipid molecules in plasma in helping to define a lipidomic signature associated with diet-induced obesity in prepubertal female pigs.

Supplemental Figure 2

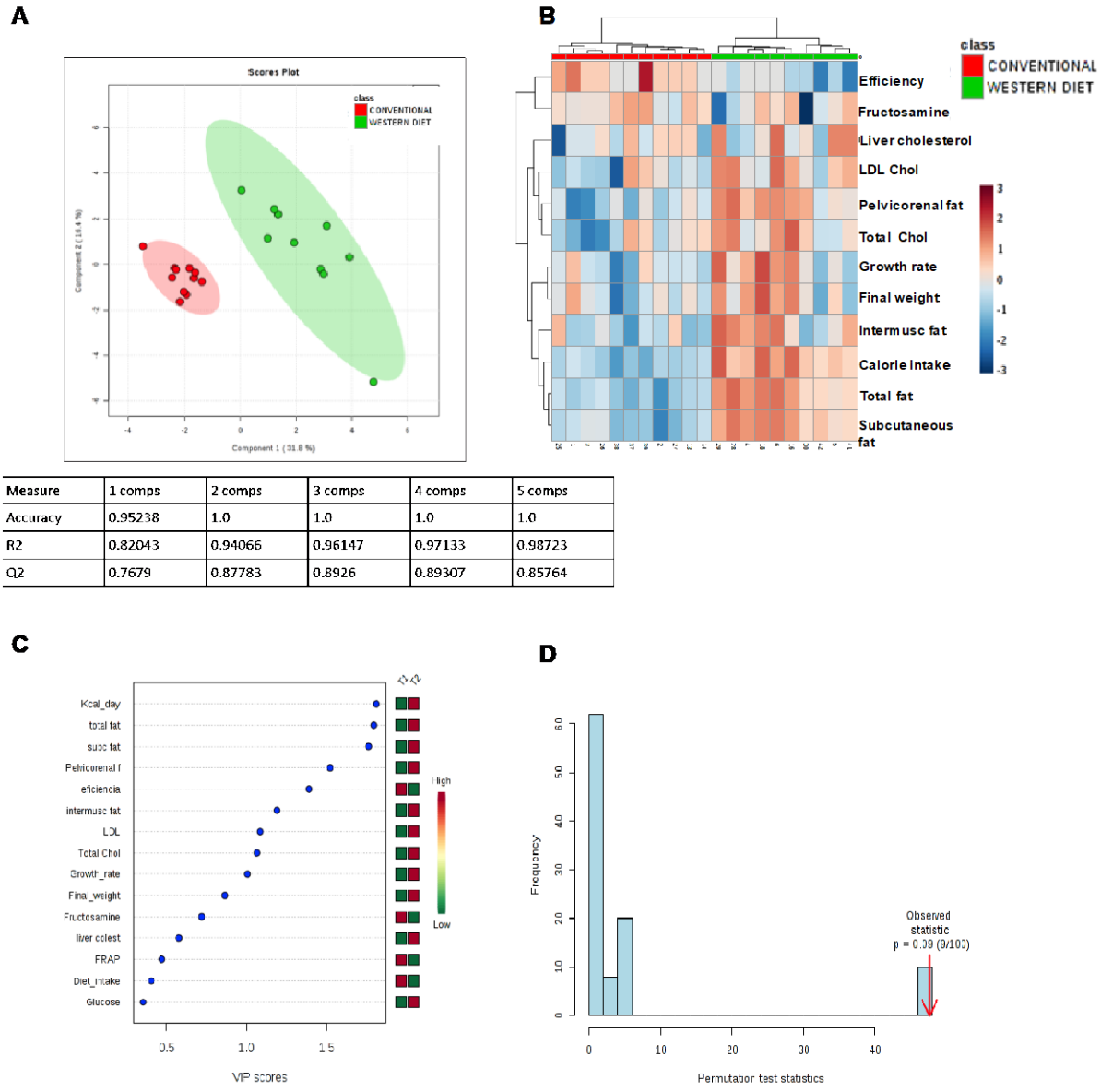

Measure	1 comps	2 comps	3 comps	4 comps	5 comps
Accuracy	0.95238	1.0	1.0	1.0	1.0
R2	0.82043	0.94066	0.96147	0.97133	0.98723
Q2	0.7679	0.87783	0.8926	0.89307	0.85764

Supplemental Figure 2. Biochemical and morphological traits define an obesity signature in the proposed model of prepubertal obesity. A) PLS-DA model demonstrating a high accuracy of the model, with more than 30% of variance being explained by the first component. B) Hierarchical clustering and heatmap shows that conventional (clinical biochemistry) and CT measures define a signature induced by western-type diet and demonstrate fat depot segregation according to anatomical location and clusterization with biochemical traits. C) Variable importance in projection (VIP) Scores of biochemical and morphological traits in the first component of the PLS-DA model. D) Permutation test of the model, showing a global p-value with a 0.09 value.

Supplemental Figure 3

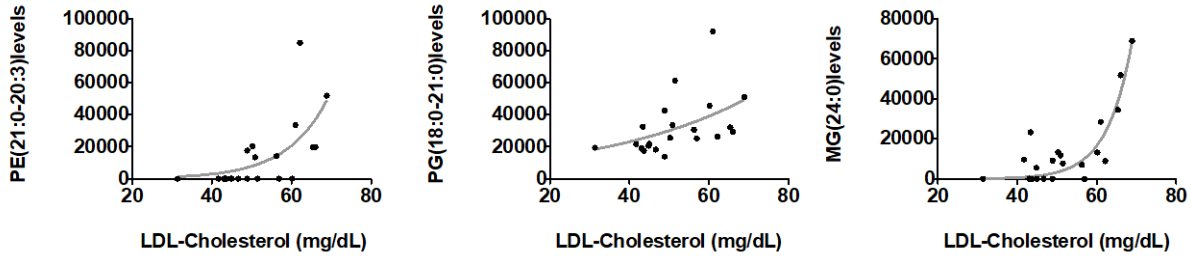

Supplemental Figure 3. Plasma LDL cholesterol values are associated with specific plasma lipids. Association of plasma concentration of selected lipids with LDL-cholesterol concentration. Shown lipids are a selection from those showing a significant correlation with specific traits (at least $p<0.05$ by Spearman's rank correlation test, see Supplemental Data for the whole list), while lines indicate non-linear fit (exponential growth equations; $Y=Y0*\exp(k*X)$).

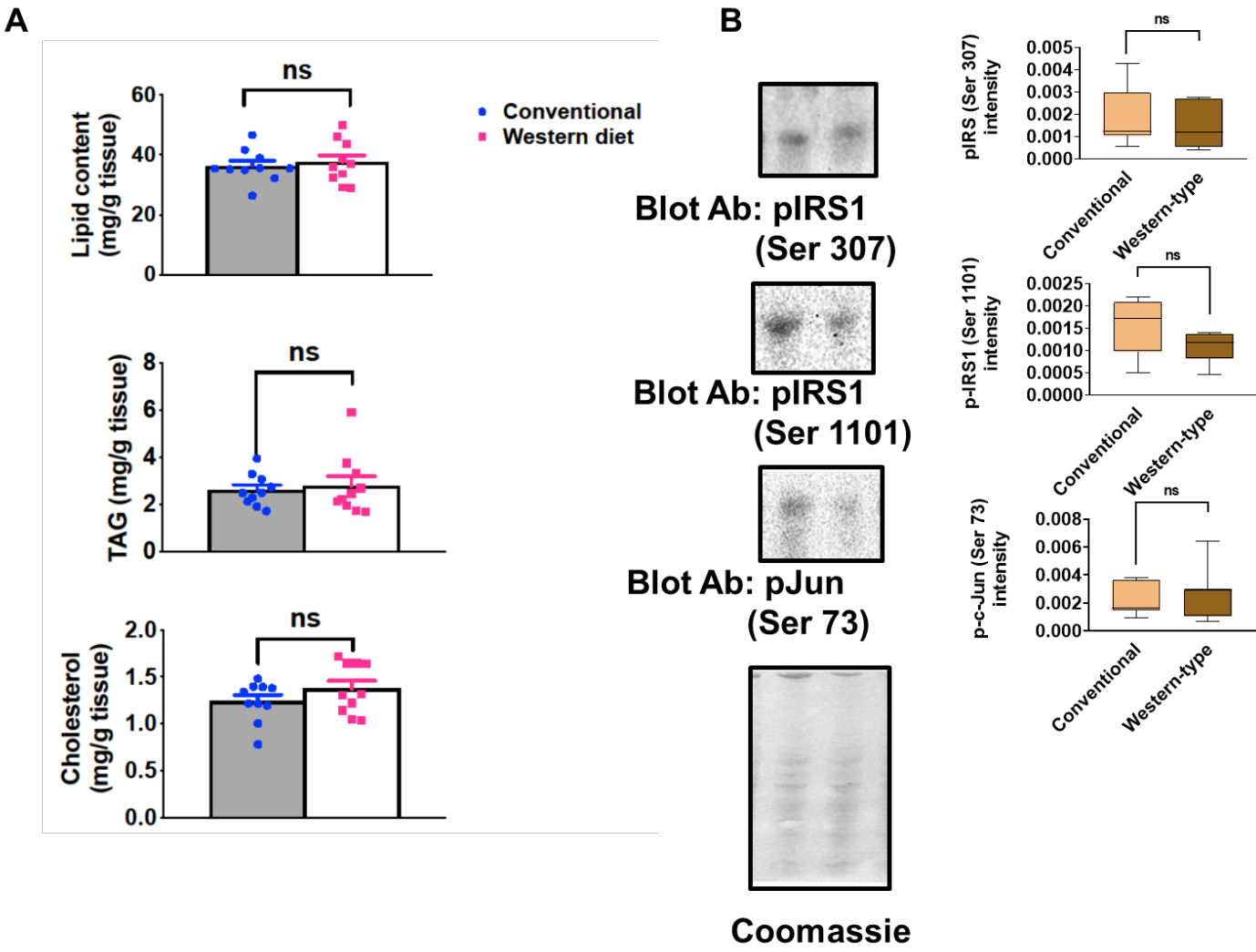

Supplemental Figure 4. A) Western-type diet does not increase lipid content in the liver, nor triacylglyceride (TAG) concentrations or cholesterol levels B) shows a representative western-blot of insulin-activity modulating signals in the liver and the influence of western-type diet. Right graphs after each blot show densitometric integrated values normalized to the total protein content, estimated by Coomassie blue staining, with p values after Students t-test (n=6 for each group)

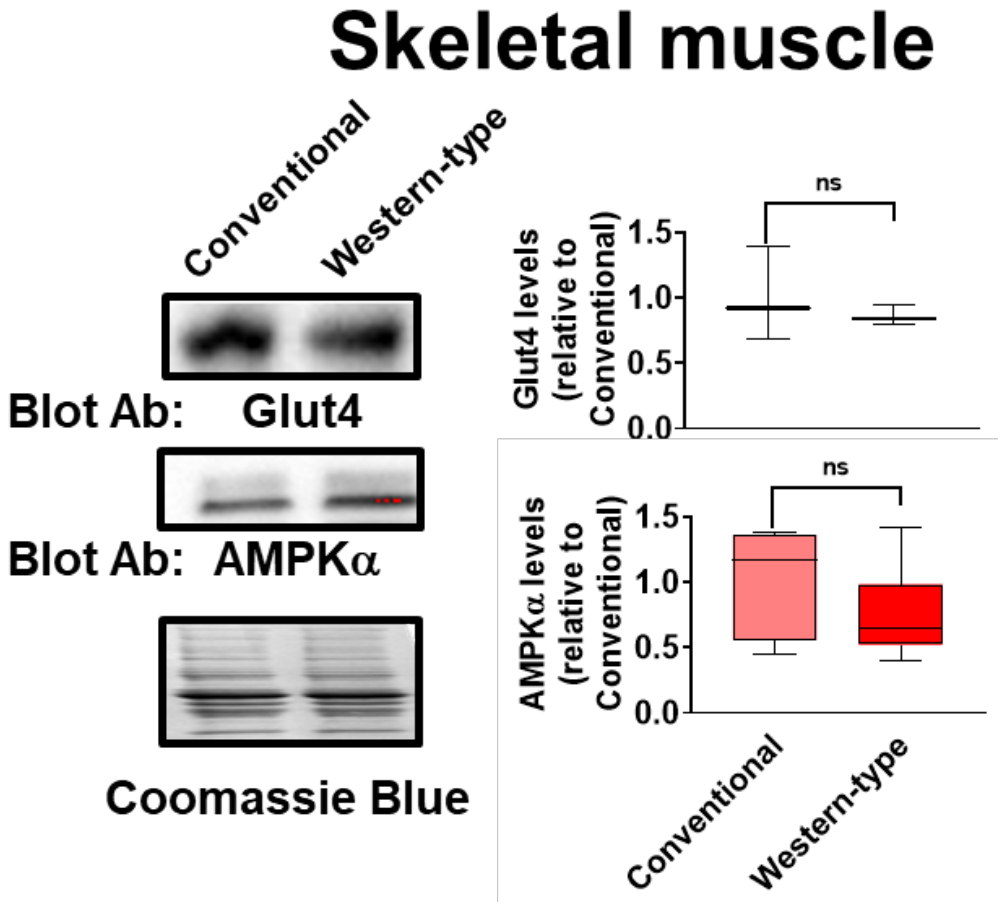

198

199 **Supplemental Figure 5. Skeletal muscle insulin-responsive signals are not affected by**
200 **the western-type diet in the prepubertal model**. Representative western-blot of insulin-
201 responsive signals in skeletal muscle. Right graphs show densitometric integrated values,
202 normalized to the intensity of animals fed with conventional diets all adjusted to total protein
203 content, estimated by Coomassie blue staining, with p values after Students t-test

Supplemental Figure 6

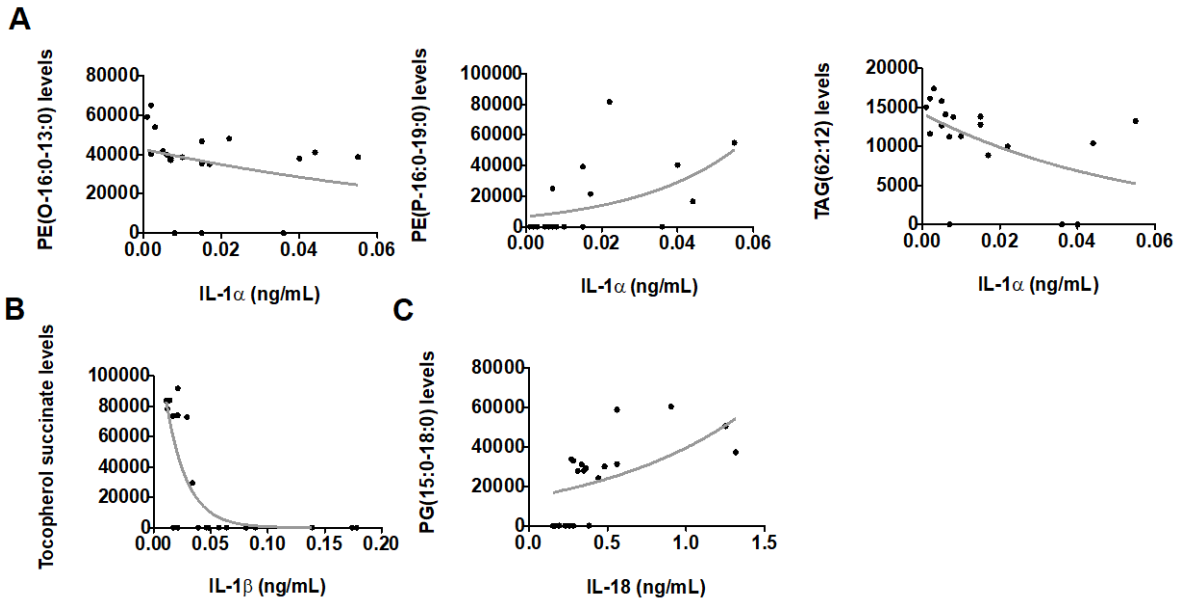

Supplemental Figure 6. Peripheral markers of inflammation are associated with specific plasma lipids. Association of plasma concentration of selected lipids with individual IL1a (A), IL1b (B) and IL-18 (C) Shown lipids are a selection from those showing significant correlation with specific traits (at least $p<0.05$ by Spearman's rank correlation test, see Supplemental Data for the whole list) while lines indicate non-linear fit (exponential growth equations; $Y=Y0*\exp(k*X)$).

211

Supplemental Figure 7

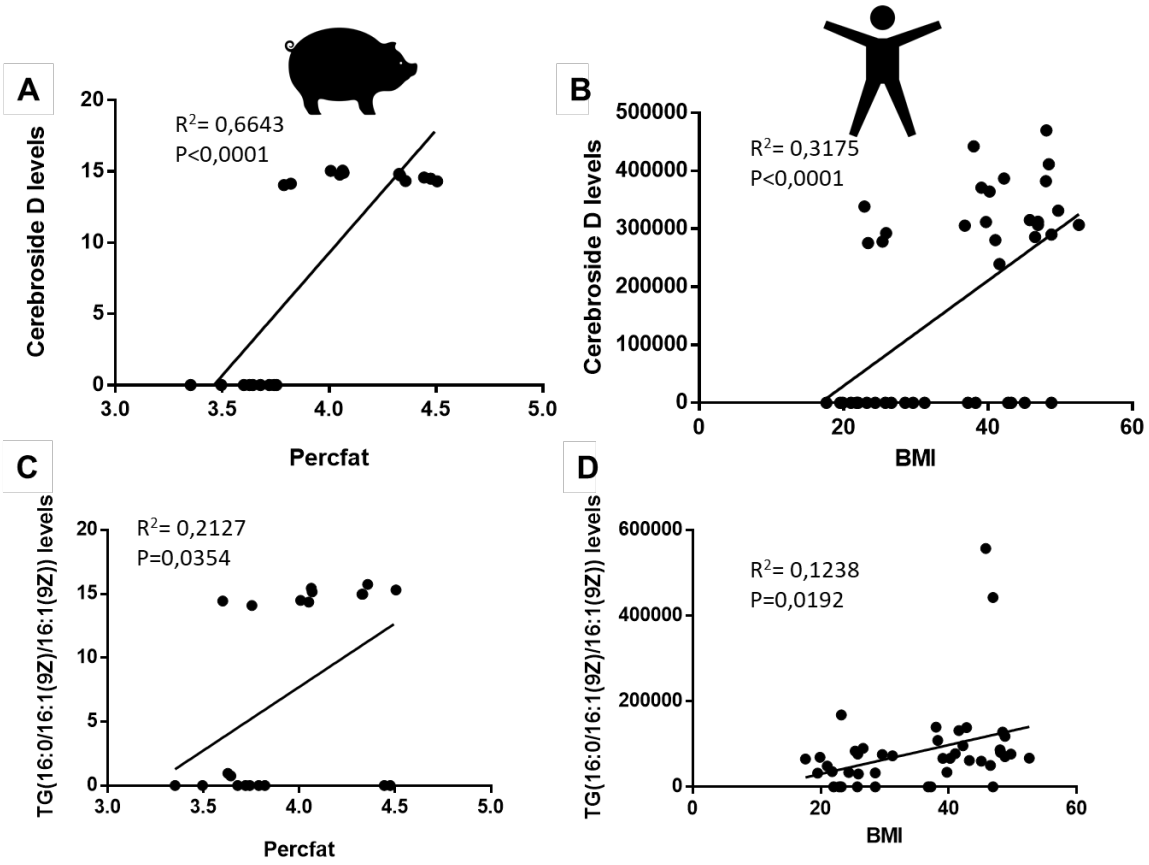

212

213 **Supplemental Figure 7.** Validation in humans with obesity of proposed biomarkers. Specific
214 lipids show a similar positive correlation with BMI (in humans, in B and D) and AT abundance
215 (in the porcine model, in A and C).. All correlations are significant (at least $p<0.05$) by
216 Spearman's rank correlation test. Lines show the linear relationship, with R^2 and p values for
217 linear adjustment shown in the inset. Pig icon comes from aLf; and Human one by Ma Qing
218 both from the Noun Project (thenountproject.com)

Supplemental Figure 8

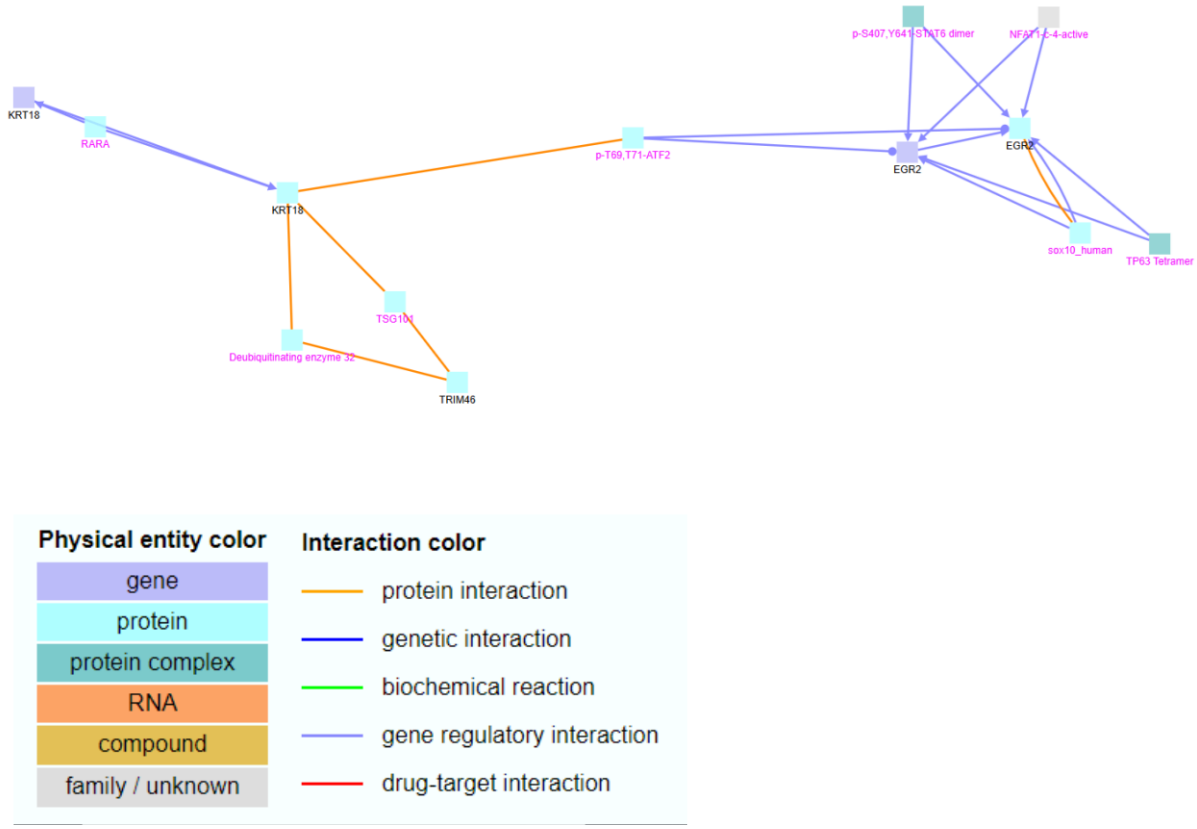

Supplemental Figure 8. Induced network module analyses of PBMC transcriptomic changes associated with the western-type diet. Genes (see main text) were entered into the ConsensusPathDB platform, and interactions, coded by colors link nodes, representing entities (identified by colors). Black node labels denote genes significantly influenced by high-calorie diet, while magenta node labels denote intermediate nodes. All types of protein interactions (high to low confidence protein interactions) were considered, as well as genetic, biochemical, and gene regulatory interactions, with all available database sources in the platform being considered.

Supplemental Figure 9

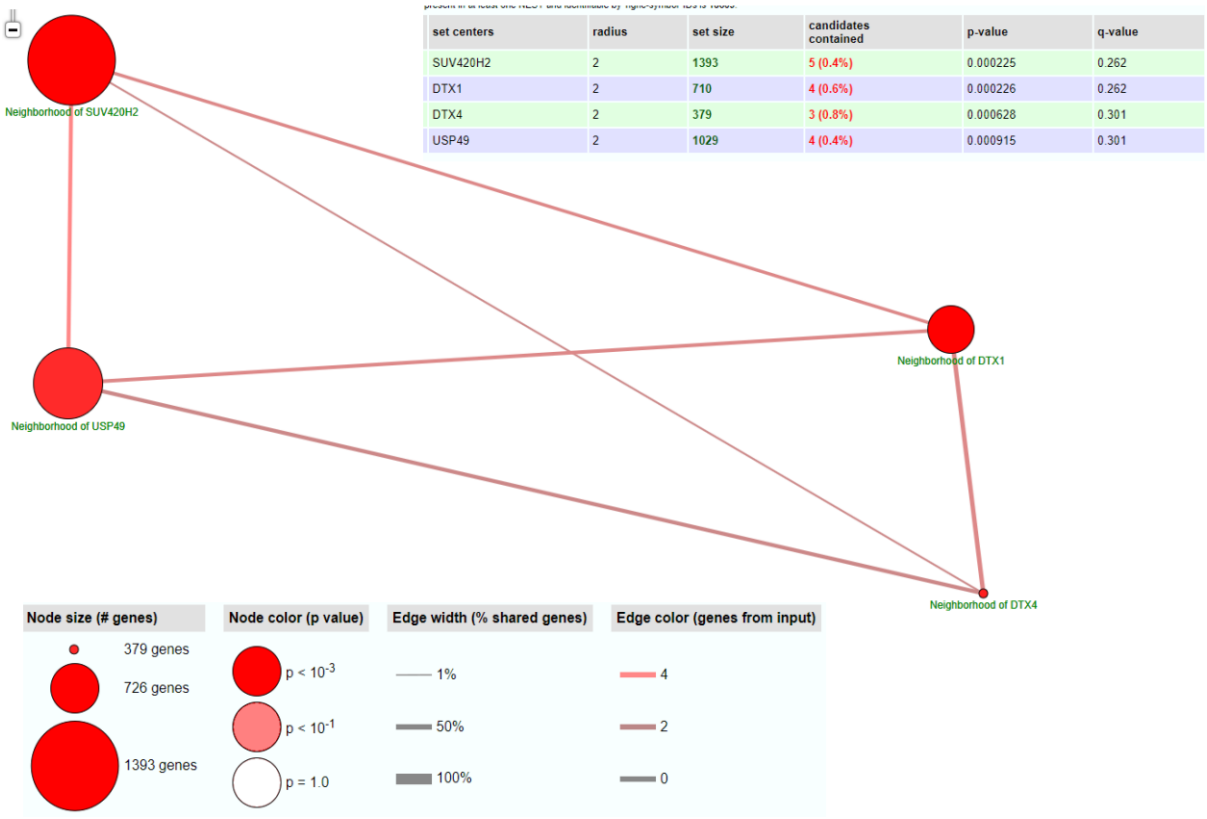

set centers	radius	set size	candidates contained	p-value	q-value
SUV420H2	2	1393	5 (0.4%)	0.000225	0.262
DTX1	2	710	4 (0.6%)	0.000226	0.262
DTX4	2	379	3 (0.8%)	0.000628	0.301
USP49	2	1029	4 (0.4%)	0.000915	0.301

Supplemental Figure 9. Network neighborhood-based entity sets of PBMC transcriptomic changes associated with western-type diet. Genes (see main text) were entered into ConsensusPathDB platform, and nodes, representing neighborhood-based entity sets (whose size is proportional to the number of genes of the set, and color intensity denotes p-value for hypergeometric tests) are linked by interactions consisting of the number of genes shared by nodes. The type of network chosen was 2-next neighbors, with a mínimum number of 2 genes from PBMC transcriptome overlap with members of the entity set (and a p<0.001 as the cutoff). The sets were obtained considering only Reactome based ones, with gene ontology level 5 categories and a p-value cutoff of 0.01 for ontology inclusión. The upper panel indicates the statistical values of each entity set.

Supplemental Figure 10

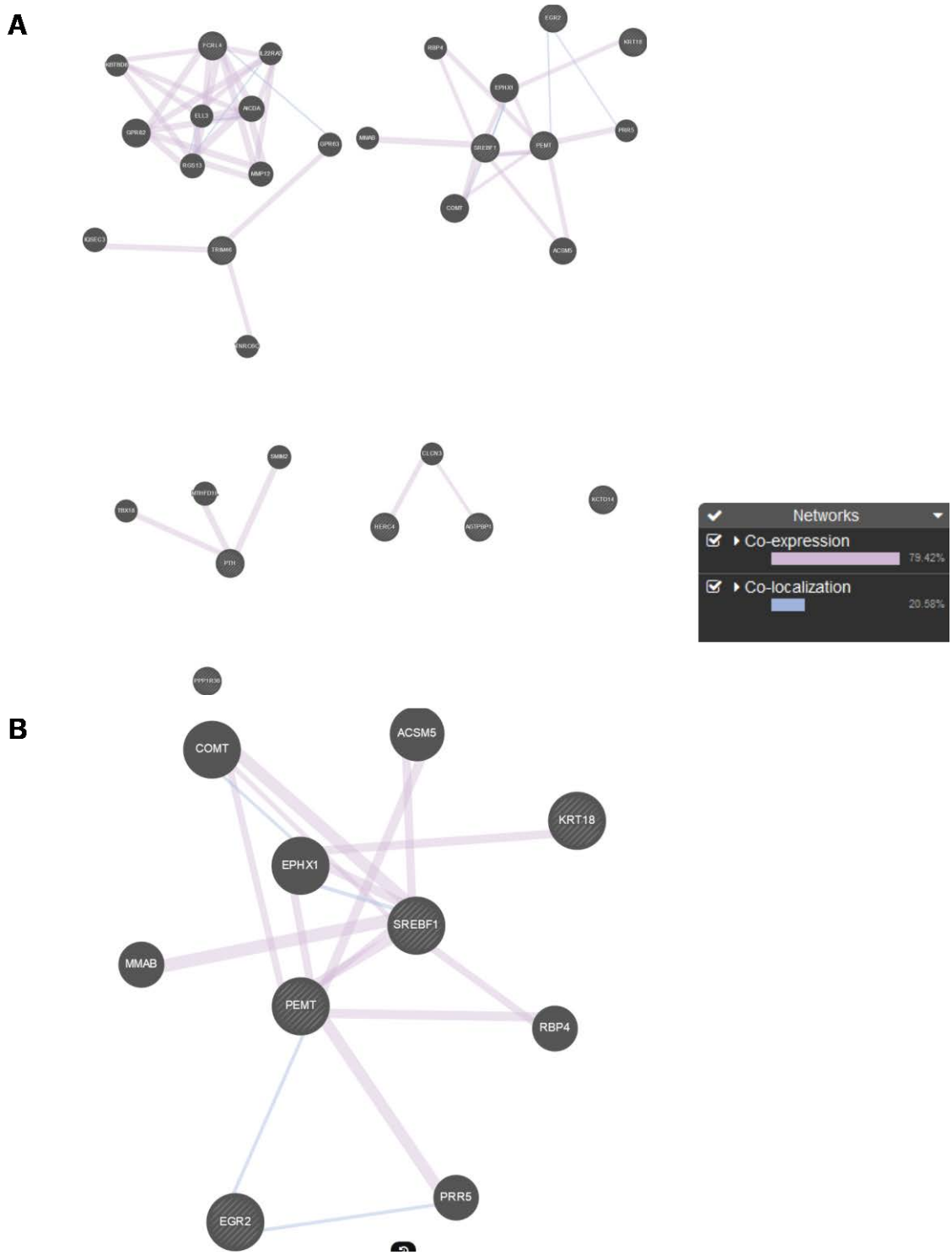

239

240

Supplemental Figure 10. Interatomic analyses of PBMC transcriptome changes. Genes whose expression was changed by western-type diet in PBMC were introduced into the Genemania platform, together with PEMT and SRBEP1, in order to evaluate its potential clustering. The results (A) show five significant co-expression networks and co-localization, with PEMT and SRBEP1 being localized into a network with EGR2 and KRT18.

Supplemental Table 1. Clinical characteristics of the cohort used for translational applicability.

Parameter	Value[1]
N	44
Age	49.41±8.71
Gender	52% female
BMI (Kg/m^2)	35.04±10.7
Waist to hip ratio	0.90±0.11
HOMA-IR	3.08±3.07
Blood Cholesterol (mg/dL)	196.2±40.35
Blood LDL-Cholesterol (mg/dL)	122.9±34.6
Blood HDL-Cholesterol (mg/dL)	54.6±15.5
Glycemia (mg/dL)	94.2±12.5
Triacylglyceridemia (mg/dL)	95.5±49.49

[1]Values shown are mean±SD unless stated otherwise.

Supplemental Table 2. Composition of experimental diets applied from 9 to 11 weeks of age

Component(%)	**Conventional transition**	**Western-type transition**
Oats	66.00	-
Wheat	-	42.00
Maize	-	16.00
Soy protein concentrate	-	-

Hydrolyzed rice protein	-	-
Caseinate	10.96	9.88
Starch	1.00	10.00
Saccharose	-	5.00
Wheat bran	15.00	4.00
Soybean hulls	4.10	-
Lard	-	10.00
Dicalcium phosphate	1.18	1.52
Calcium carbonate	0.98	0.51
Salt	0.35	0.37
L-Lysine-HCl	-	0.19
L-Threonine	-	0.03
DL-Methionine	-	0.10
L-Tryptophan	-	-
Ethoxiquin	0.02	0.02
Vit-Min complex (*)	0.40	0.40

(*) Provides per kg feed: vitamin A (E-672) 5500 UI; vitamin D3 (E-671) 1100 UI; vitamin E (alfa-tocopherol) 7 mg; vitamin B1 0.5 mg; vitamin B2 1.4 mg; vitamin B6 1 mg; vitamin B12 8 µg; vitamin K3 0.5 mg; calcium panthotenate 5.6 mg; nicotinic acid 8 mg; choline 120 mg; Fe (E-1) (from FeSO4·7H2O) 80 mg; I (E-2) (from Ca(I2O3)2) 0.5 mg; Co (E-3) (from 2CoCO3·3Co(OH)2·H2O) 0.4 mg; Cu (E-4) (from CuSO4·5H2O) 5 mg; Cu (E-4) (from amino acids quelate) 5 mg; Mn (E-5) (from MnO) 40 mg; Zn (E-6) (from ZnO) 100 mg; Se (E-8) (from Na2SeO3) 0.25 mg.

Supplemental Table 3. Nutritional composition of experimental diets applied from 9 to 11 weeks of age

Amount (%)	**Conventional transition**	**Western-type transition**
Crude Protein	17.98	15.55
Crude Fibre	12.20	1.68
Fat	4.98	11.80
Ash	5.96	4.15

Sodium	0.15	0.15
Chloride	0.29	0.31
Total calcium	0.86	0.70
Total phosphorous	0.58	0.49
Digestible phosphorous	0.27	0.27
Lysine	1.11	1.03
Threonine	0.75	0.65
Methionine	0.41	0.44
Met+Cys	0.69	0.64
Tryptophan	0.26	0.22
Energy (MJ ME/kg)	10.42	15.39

263

264 **Supplemental Table 4**. Composition of experimental diets applied from 12 to 19

265 weeks of age

Component(%)	Conventional	Western-type
Oats	55.28	-
Wheat	-	45.87
Maize	-	13.56
Caseinate	9.76	8.54
Starch	13.13	10.00
Saccharose	-	5.00
Wheat bran	15.00	4.00
Soybean hulls	4.00	-
Lard	-	10.00
Dicalcium phosphate	1.27	1.51

Calcium carbonate	0.78	0.51
Salt	0.36	0.37
Ethoxiquin	0.02	0.02
L-Lysine-HCL	-	0.15
L-Threonine	-	0.01
DL-Methinonine	0.003	0.07
Vit-Min complex (*)	0.40	0.40

(*) Provides per kg feed: vitamin A (E-672) 5500 UI; vitamin D3 (E-671) 1100 UI; vitamin E (alfa-tocopherol) 7 mg; vitamin B1 0.5 mg; vitamin B2 1.4 mg; vitamin B6 1 mg; vitamin B12 8 µg; vitamin K3 0.5 mg; calcium panthotenate 5.6 mg; nicotinic acid 8 mg; choline 120 mg; Fe (E-1) (from FeSO4·7H2O) 80 mg; I (E-2) (from Ca(I2O3)2) 0.5 mg; Co (E-3) (from 2CoCO3·3Co(OH)2·H2O) 0.4 mg; Cu (E-4) (from CuSO4·5H2O) 5 mg; Cu (E-4) (from amino acids quelate) 5 mg; Mn (E-5) (from MnO) 40 mg; Zn (E-6) (from ZnO) 100 mg; Se (E-8) (from Na2SeO3) 0.25 mg.

Supplemental Table 5. Nutritional composition of experimental diets applied from 12 to 19 weeks of age

Amount(%)	Conventional	Western-type
Protein	17.6	14.34
Fat	4.6	11.55
Fiber	11	1.72
Sodium	0.15	0.15
Chloride	0.29	0.31
Calcium	0.80	0.70
Total phosphorous	0.56	0.49
Digestible phosphorous	0.27	0.27
Lysine	0.99	0.90
Threonine	0.66	0.57
Methionine	0.36	0.37
Met+Cys	0.61	0.56
Tryptophan	0.23	0.20
Ash	5.55	4.13
Energy (MJ/ kg)	10.83	15.16

278

279 **Supplemental Table 6.** Antibodies and conditions.

280

Antigen	Supplier	Reference	Dilution
GLUT2	Abcam	ab104622	1:1000
SREBP1	Abcam	ab3259	1:1000
GLUT4	Invitrogen	MA1-83191	1:1000
AMPKα	Invitrogen	PA5-17398	1:1000
Phospho-IRS1 (Ser 307)	Upstate	07-247	1:1000
Phospho-IRS1 (Ser 1101)	Cell Signaling	2385	1:300
Phospho-c-JUN (Ser73)	Cell Signaling	3270	1:1000
anti-mouse IgG	Amersham	NA931V	1:30000
anti-rabbit IgG	Pierce	31460	1:100000

281

282

283 **Supplemental Table 7**. Internal standards for lipidomic analyses.

284

Compound	Reference		
1,3(*d*5)-dihexadecanoyl-glycerol	110537, Avanti Lipids	Avanti	Polar
1,3(*d*5)-dihexadecanoyl-2-octadecanoyl-glycerol	110543, Avanti Lipids	Avanti	Polar
1-hexadecanoyl(*d*31)-2-(9Z-octadecenoyl)-sn-glycero-3-phosphate	110920, Avanti Lipids	Avanti	Polar
1-hexadecanoyl(*d*31)-2-(9Z-octadecenoyl)-sn-glycero-3-phosphocholine	110918, Avanti Lipids	Avanti	Polar
1-hexadecanoyl(*d*31)-2-(9Z-octadecenoyl)-sn-glycero-3-phosphoethanolamine	110921, Avanti Lipids	Avanti	Polar
1-hexadecanoyl-2-(9Z-octadecenoyl)-sn-glycero-3-phospho-(1'-rac-glycerol-1',1',2',3',3'-*d*5)	110899, Avanti Lipids	Avanti	Polar
1-hexadecanoyl(*d*31)-2-(9Z-octadecenoyl)-sn-glycero-3-phospho-myo-inositol	110923, Avanti Lipids	Avanti	Polar
1-hexadecanoyl(*d*31)-2-(9Z-octadecenoyl)-sn-glycero-3-[phospho-L-serine]	110922, Avanti Lipids	Avanti	Polar
26:0-*d*4 Lyso PC	860389, Avanti Lipids	Avanti	Polar
18:1 Cholesterol (*d*7) ester	111015, Avanti Lipids	Avanti	Polar
cholest-5-en-3ß-ol(*d*7)	LM-4100, Avanti Lipids	Avanti	Polar

D-erythro-sphingosine-*d*7	860657, Avanti Polar Lipids
D-erythro-sphingosine-*d*7-1-phosphate	860659, Avanti Polar Lipids
N-palmitoyl-*d*31-D-erythro-sphingosine	868516, Avanti Polar Lipids
N-palmitoyl-*d*31-D-erythro-sphingosylphosphorylcholine	868584, Avanti Polar Lipids
Octadecanoic acid-2,2-*d*2	19905-58-9, Sigma Aldrich

285

286

287

288 **Supplemental Table 8** . Changes in subcutaneous AT mRNA concentration induced

289 by the western-type diet.

290

Gene	Conventional[1]	Western-type	Change (%)	p-value
lep	0.0225 ± 0.0152	0.064 ± 0.0215	184.8	<0.00001
Il6	0.0072 ± 0.0079	0.0032 ± 0.0015	-55.7	0.15
Irs1	0.0635 ± 0.0291	0.0464 ± 0.0199	-26.9	0.158
fasn	5.4763 ± 1.732	5.5608 ± 1.4093	1.5	0.908
adipoq	126.87 ± 71.05	94.71 ± 34.74	-25.3	0.211
Insr1	1.05 ± 0.22	1.13 ± 0.22	7.6	0.455
gapdh	17.77 ± 4.53	20.9 ± 7.29	17.6	0.247

291 [1]Values shown are mean±SD unless stated otherwise.

292

293

Supplemental Table 9. Changes in plasma interleukine concentration induced by the western-type diet.

Parameter (pg/mL)	Conventional	Western-type	p[1]
IL-1a	0.016.9±0.014	0.014±0.019	0.9
IL-1b	0.054±0.047	0.056±0.061	0.9
IL-1ra	0.13±0.12	0.11±0.11	0.6
IL-10	0.08±0.12	0.09±0.16	0.9
IL-18	0.43±0.31	0.48±0.36	0.9

Values shown are mean±SD unless stated otherwise. [1]Student's t-test comparison between values in conventional and western-type diets

Supplemental Table 10. Changes in plasma metabolome induced by western-type diet

Compound	Log FC	p	p (Corr)	Regulation (Conventional versus western-type)	FC (Control vs High Calorie)
Leucine	-0.44	8.22E-04	2.73E-02	Up	1.36
Pantheine	-1.35	1.51E-04	8.38E-03	Up	2.55
N-ethylarachidonoyl amine	-14.73	2.16E-04	1.09E-02	Up	27116.81
N-Lignoceroylsphingosine	-0.94	9.37E-04	3.01E-02	Up	1.92
3alpha,6alpha,7alpha,12alpha-Tetrahydroxy-5beta-cholest-24-en-26-oic acid	13.93	1.30E-05	9.63E-04	Down	-15602.22
GlnMetGln	14.47	4.82E-08	6.85E-06	Down	-22617.46

Figure 2 whole western blots

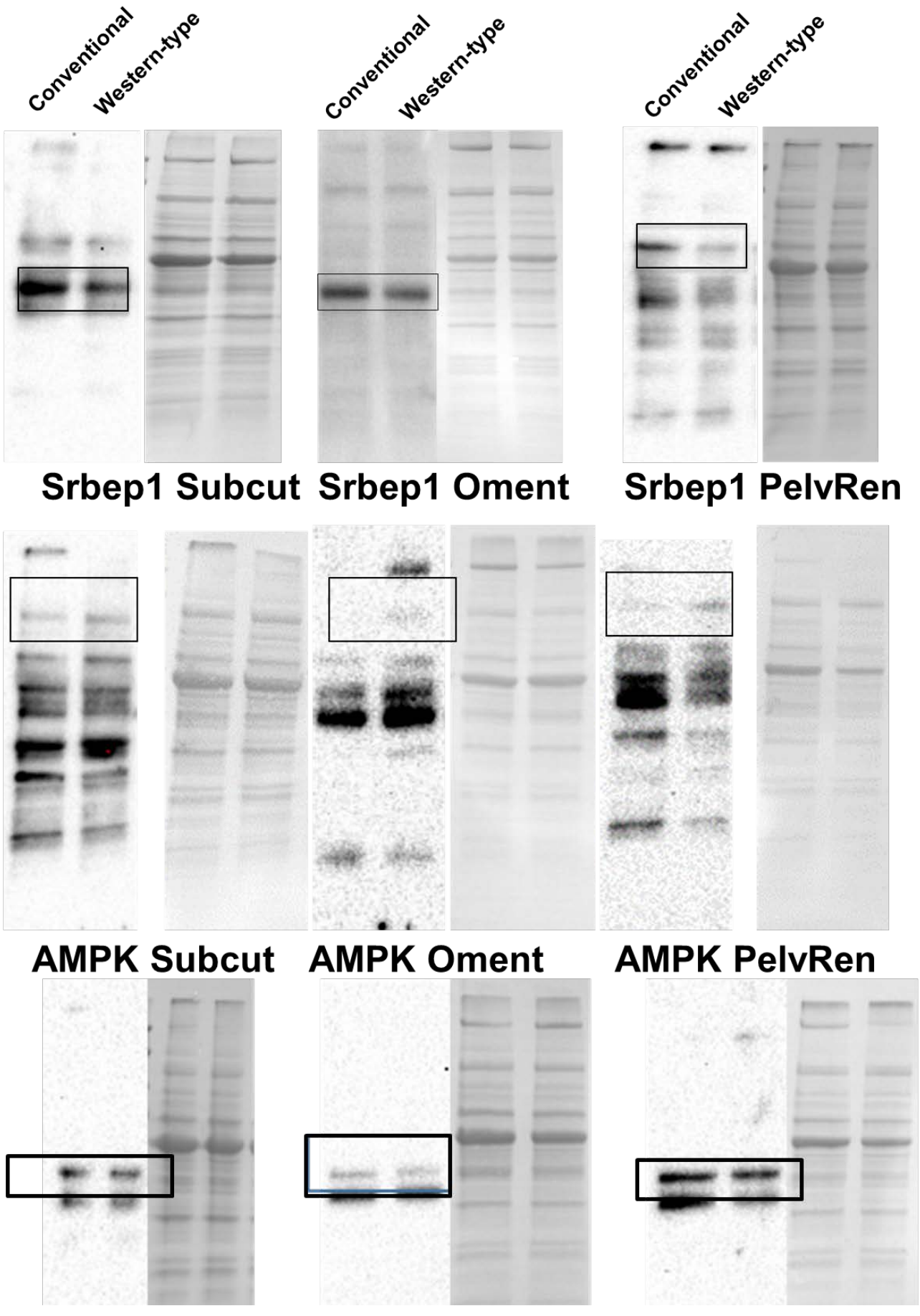

Figure 4 whole western blots

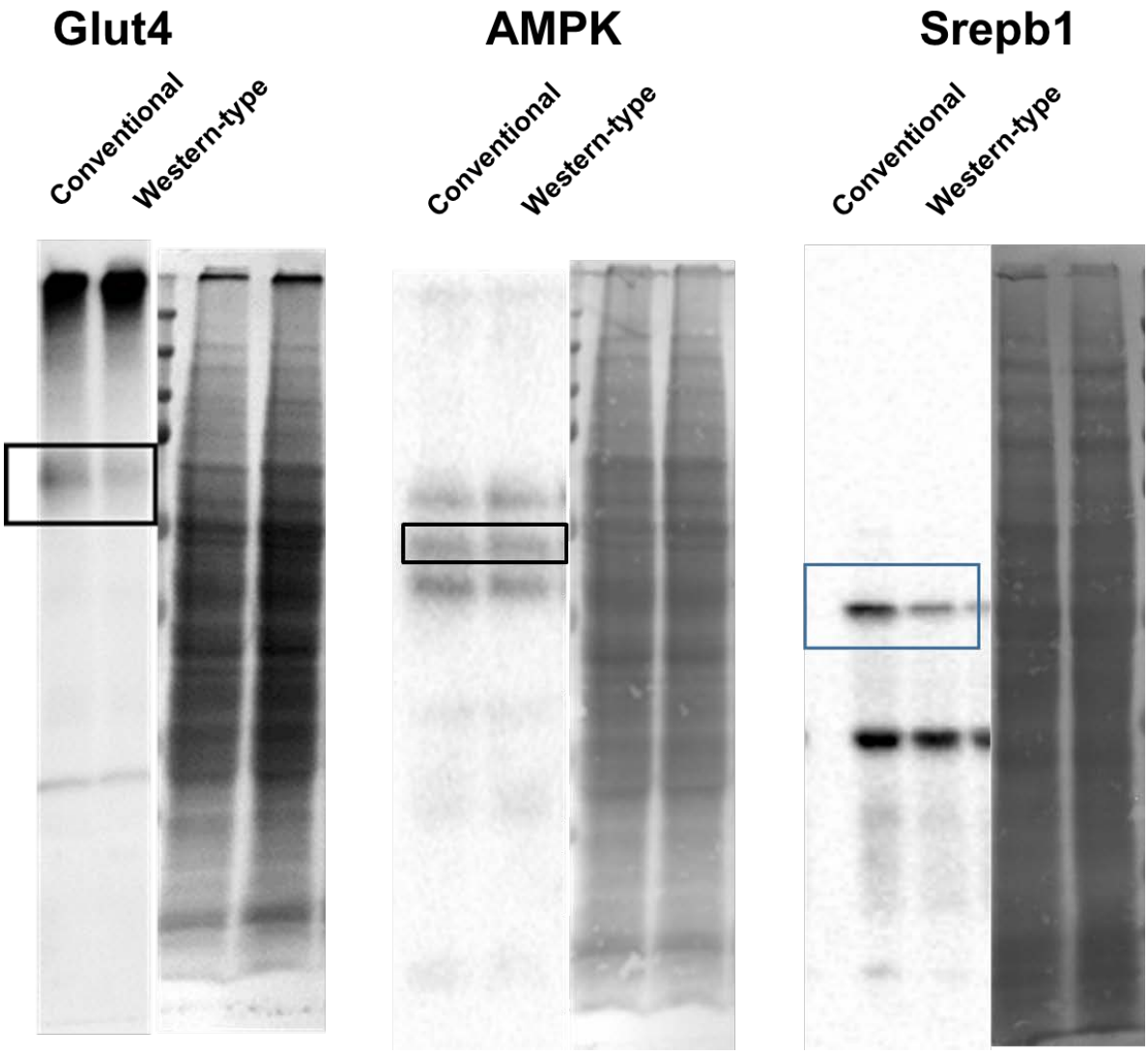

306

Supplemental Figure 4 whole western blots

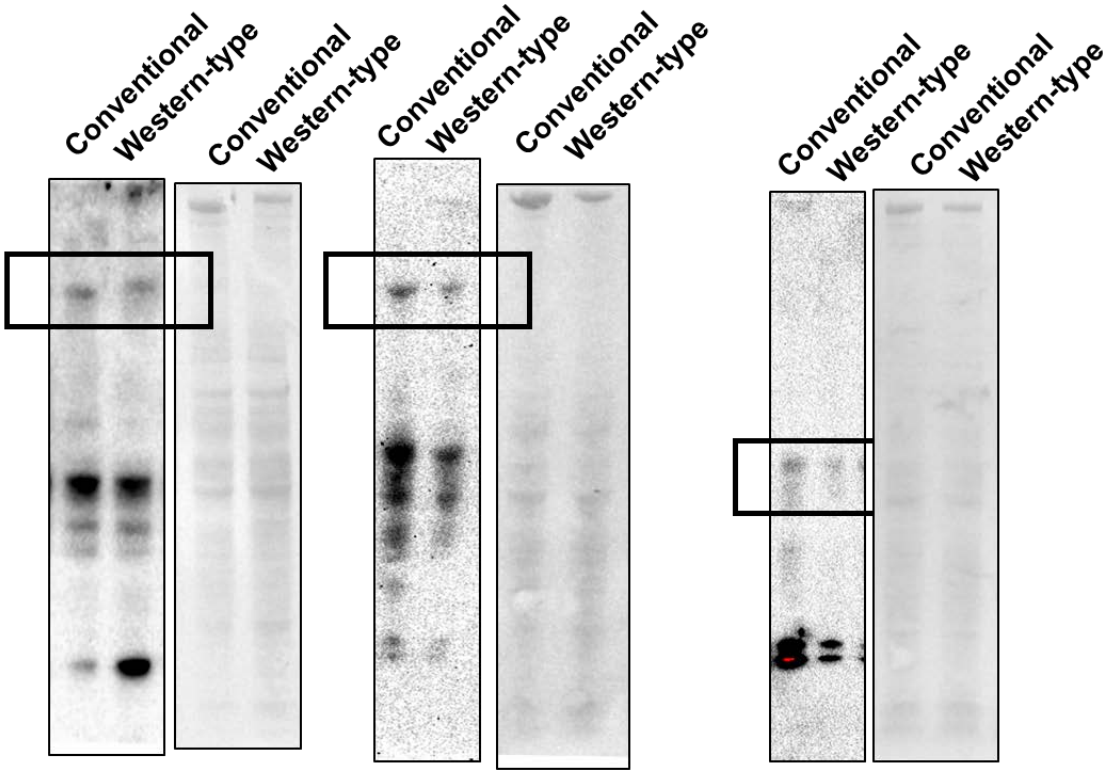

307

Supplemental Figure 5 whole western blots